

ORBITER ENTRY HEATING LESSONS LEARNED FROM
DEVELOPMENT FLIGHT TEST PROGRAM

J. W. Haney
Space Transportation and Systems Group
Rockwell International
Downey, California

SUMMARY

The Space Shuttle orbiter's thermal protection system (TPS), designed mainly on the basis of wind tunnel test data, has successfully completed its design, development, and flight test program. The flight test data provide an exceptional opportunity to evaluate the use of wind tunnel test data for the design of TPS for reentry vehicles. Comparisons of flight test data against wind tunnel data used to design the orbiter's TPS have been developed. These flight data, though still in the preliminary analysis phases, generally support the use of wind tunnel test data in the design of TPS for hypersonic reentry vehicles.

INTRODUCTION

At the onset of the design of the orbiter's TPS, wind tunnel data were relied upon heavily to develop aerothermodynamic prediction methods. These methods, either semiempirical correlations or validated analytical methods, were extrapolated to flight conditions in conjunction with an uncertainty analysis. Today, the process of methods verification based on flight test data has begun (figure 1).

This paper compares reentry flight test data from the first five flights of the Space Shuttle Columbia with the wind tunnel test data used to predict the environments on which the TPS design was based. In the process, basic design heating methods will be explained. The types of reentry missions on which data were obtained, instrumentation types and locations, and some current problems with available flight data are discussed. Differences between flight and wind tunnel test data are analyzed. Emphasis is placed on the orbiter leeside.

SYMBOLS

| | |
|---|---|
| h | heat transfer coefficient |
| H | enthalpy |
| L | fuselage reference length (1,284.3 in.) |
| P | pressure |

| | |
|------------|--|
| Pr | Prandtl number |
| Re | Reynolds number |
| ST | Stanton number |
| T | temperature |
| V | velocity |
| X | axial length |
| α | angle of attack |
| β | angle of sideslip |
| δ | control surface deflection |
| θ^* | flow angle (body angle plus angle of attack) |
| μ | viscosity |
| ρ | density |

Subscripts:

| | |
|----------|---------------------|
| BF | body flap |
| E | elevon |
| e | boundary layer edge |
| FP | flat plate |
| o | stagnation |
| r | recovery |
| TR | transition |
| w | wall |
| θ | momentum thickness |
| ∞ | free stream |

DESIGN HEATING APPROACH

Over a period of almost 12 years, from the start of the Phase A studies to the first orbital flight test (OFT) of Columbia, 50 wind tunnel tests (approximately 5,200 hours) were conducted for the purpose of developing aerothermodynamic math

models to estimate entry heating environments. Through the course of this testing, configuration features were finalized, different facilities were investigated, and a large number of heating parameters were varied (figure 2). Even with all of this testing, the ability to directly simulate an entry trajectory was limited (figure 3). High Mach number with associated low Reynolds numbers were beyond the capability of wind tunnels. This inability to simulate was rationalized by the belief that correlations developed for lower Mach numbers (approximately 8) and higher Reynolds numbers could be accurately applied to other flight conditions.

Two different approaches were taken to utilize wind tunnel test data for environment definition. One approach, the simple geometric theory, was employed mainly on the orbiter lower surfaces. The other approach, wind tunnel data taken directly, was applied to the leeward surfaces.

The simple geometric theory approach subdivided the orbiter into simple shapes (spheres, cylinders, wedges, and cones) for which standard analytical solutions were in existence (figure 4). These simple geometric theories (mainly wedges and flatplates) were adjusted to match wind tunnel test data. The adjustments from the standard Eckert reference enthalpy flatplate solutions were to take into account such variations as streamline divergences and flow running lengths. These adjustment factors, developed for both laminar and turbulent boundary layers in the wind tunnel, were held constant when extrapolating to flight conditions.

The direct application of wind tunnel data for the upper surfaces was obtained by correlations of wind tunnel data (in terms of a nondimensional local film coefficient to that of a 1-ft-radius sphere) as a function of angle of attack, angle of sideslip (yaw), free-stream Reynolds number, and free-stream Mach number (figure 5). This essentially correlates the orbiter leeside into blunt body relationships. Regions of vortex scrubbing and flow impingement were allowed to vary somewhat beyond the wind tunnel values based on local pressure levels.

In addition to the basic use of wind tunnel test data, uncertainties were accounted for in order to have a conservative heating estimate for assessment of the first flight. Some conservatism was inherent in the analysis, such as assuming a fully catalytic surface. Other uncertainties were knowingly added (see figure 6). Uncertainties were determined individually by either analysis of wind tunnel data or by theoretical assumptions. These uncertainties were root sum squared together to obtain the final uncertainty values.

FLIGHT TEST DATA

The Space Shuttle orbiter development test program consisted of four test flights. However, problems in obtaining flight test data resulted in the addition of a fifth instrumented flight. The entry trajectories were shaped to be benign from an induced thermal point of view, with each flight having a vehicle angle of attack of 40 deg throughout most of the entry (figure 7). Emphasis was placed on maintaining adequate structural temperature margins. All five trajectories were similar, though STS-3 and STS-4 flights had slightly increased surface temperatures and reduced entry flight time.

Aerothermodynamic test data were obtained by three means: surface thermocouples, calorimeters, and surface pressure taps (figures 8a, 8b, and 8c).

Thermocouples were to be installed slightly below the outer mold line (OML) of the TPS. However, X-rays of tiles used in TPS certification testing indicated that the position of the thermocouple below the OML was not always constant. This was especially true of the felt reusable surface insulation (FRSI) located on the upper surfaces. Similarly, calibration of thermocouples on Columbia has indicated variations in response to a known induced environment. This condition becomes critical in assessing transient variations in environments and is currently being incorporated into the data analysis and verification process. This variation in response has been related to a variation in the effective depth of the thermocouples from the OML. All data presented in this paper considered the thermocouples to be reading surface temperature. These data will need to be adjusted once the effective depth or thermal math model of each thermocouple has been ascertained.

Calorimeters, used as a means of gathering data, were essentially available for only the first two development flights. The unanticipated responses of the calorimeters late in the STS-1 trajectory led to the removal of most and to their replacement with surface thermocouples. Unfortunately, after analyzing five flights of test data, the calorimeters appear to have been providing useful data during the first two test flights. The calorimeters, more sensitive than surface thermocouples, were quite responsive to vehicle attitude changes; however, the overall magnitude of the calorimeter readings remains in question.

Several unfortunate flight data problems reduced the total amount of available data so that only three entire flights of thermocouple, two entire flights of pressure, and one entire flight of calorimeter data were obtained during the OFT program. Partial data were obtained on both the first and fourth test flights.

FLIGHT TEST RESULTS

Lower Surface

In examining flight test data on the orbiter lower surfaces, three major statements can be made: (1) noncatalytic effects were present, (2) boundary layer transition occurred later than predicted, and (3) local pressures generally agreed with theory.

The noncatalytic effects not accounted for in the TPS design appear to be the most conservative element in that design. Figure 9 shows the differences between equilibrium (fully catalytic) and flight test data at two locations on the orbiter lower-surface centerline. Also evident is the agreement between the Spalding and Chi turbulent theory and flight data. Detailed discussions of noncatalytic effects are found in reference 1.

Roughness-induced boundary layer onset transition criterion was conservative for the first test flight; however, the TPS was actually designed based on a smooth-body criterion. Flight data indicate that transition occurs somewhat sooner than

predicted by the smooth-body criterion developed from wind tunnel test data (figure 10). Detailed discussions of boundary layer transition and the orbiter may also be found in reference 1.

The local pressure levels (low-pressure gradient regions) on the orbiter lower surfaces were based on correlations of P_L/P_∞ as a function of free-stream Mach number, angle of attack, and local geometric angle. These correlations initially determined based on wedge and cone data were modified using orbiter wind tunnel test data, so that

$$P_L/P_\infty = 0.2397 + 1.161 M_\infty \sin\theta^* + 1.060 (M_\infty \sin\theta^*)^2 + 0.0487 (M_\infty \sin\theta^*)^3$$

This approach provided excellent agreement with flight test data (figure 11).

Heating to the wing leading edge described in a separate paper (reference 2) can be summarized as follows. Outside of the shock impingement region, flight data agree well with the methods developed based on wind tunnel data; inside of the shock-influenced region, flight data were higher than wind-tunnel-based data.

Upper Surface

The main emphasis of this paper is the comparison of flight and wind tunnel data for the orbiter upper surfaces. Specifically, the fuselage side, payload bay door, wing upper surface, vertical tail, and orbital maneuvering system (OMS) pod will be discussed in this section. The wind tunnel test data used for comparisons with flight data are taken from references 3 through 10.

Fuselage Side

The flow on the orbiter fuselage side, as well as on many upper surface regions, is generally characterized by a separated flow region interrupted by vortex scrubbing (figure 12). The vortex is believed to develop from the junction of the wing glove and the fuselage side, and it traverses along the fuselage side at an angle similar to the vehicle angle of attack. This vortex scrubs the vertical surfaces of the fuselage and payload bay doors as indicated in figure 12. Once outside of the vortex zone, the heating drops rapidly to separation values. Derived from wind tunnel test data, the vortex location and strength were determined to be sensitive to angle of attack, yaw, and Reynolds number. The effects of varying these parameters in the wind tunnel were to shift the vortex forward or aft along the fuselage side.

In the regions of nonvortex attached flow (i.e., forebody side), flight data and wind tunnel data are in general agreement. In the wind tunnel, nondimensionalized heat transfer data in these same regions were insensitive to variations in Reynolds number and somewhat insensitive to angle of attack, which is indicative of laminar attached flow. There appears to be, however, some evidence of noncatalytic effects as seen on the lower surface in regions just aft of the nose cap (figure 13).

Moving aft along the side, at 30-percent body length, the agreement between flight and wind tunnel data is excellent in the range of Reynolds numbers tested in the wind tunnel (figure 14). For the case when Reynolds numbers are less than those tested in the wind tunnel, the heating is less than predicted. Above the Reynolds number limit of the wind tunnel, heating is generally equal to or greater than predictions. Wind tunnel data were not always correlated exactly when developing aeroheating math models. The correlation procedure (figure 5) sometimes did not lend itself to certain variations between parameters or physical locations. This is evident in figures 14b and 14c.

In regions strongly influenced by vortex scrubbing, the wind tunnel data underpredict flight test data (figure 15). The differences increase as the Reynolds numbers increase. The exact causes of this underprediction are not quite understood at present, but are believed to be related to the differences in specific heat ratios between wind tunnel and flight (1.4 versus 1.2). This difference should result in moving the vortex closer to the sidewall and increase the influence on heating. The other noticeable difference in flight data is the rapid rise in the temperature (heating rate) at a Reynolds number of approximately 2.0×10^6 . This rise is quite evident with the $\alpha = 40$ deg data and can be implied with the limited $\alpha = 35$ deg and $\alpha = 30$ deg data. This rise in temperature reaches a level that is somewhat consistent with that of the lower angles of attack (an increase of 400 to 600 percent, figures 15b and 15c). The flow appears to be departing from a weak vortex and separated condition to that of a strong vortex and attached interaction.

Further aft on the orbiter's side (also strongly influenced by the vortex) is a region that, in the wind tunnel, did not experience any noticeable vortex scrubbing (figure 16). The flow in this region was separated at $\alpha = 40$ deg in the wind tunnel, but under flight conditions it experiences vortex scrubbing. Again note the rapid change in heating level at a Reynolds number of 2.0×10^6 .

Payload Bay Door

In the wind tunnel, the flow on the payload bay doors was characterized by a pair of weak vortices traversing along the top of the doors; however, in flight these vortices do not appear to be attached at the high angle of attack, $\alpha = 40$ deg. During the TPS design phase of the Shuttle, much effort was made to correlate the wind tunnel test data on the payload bay doors. The correlating parameter used was Stanton number based on free-stream conditions. When this parameter is used for both flight and wind tunnel data, it can be seen that as the vehicle angle of attack is reduced, the differences between flight and wind tunnel are reduced (figures 17a, 17b, and 17c). Interestingly, Apollo and Shuttle leeside data are in general agreement for certain flight conditions (figure 18).

With the payload bay door wind tunnel data coming into better agreement for reduced angles of attack, this points to the need to maintain a view of the entire orbiter when extrapolating vehicle capability to more severe entries.

Wing Upper Surface

Of all the regions on the orbiter, the area most overpredicted by wind tunnel data was the wing upper surface. Wind tunnel data had indicated some vortex

scrubbing on the outboard portion of the wing at a 40-deg angle of attack, with more severe scrubbing at the lower angles of attack. Analysis of oil flow data had indicated that this vortex was associated with the interaction of the bow and leading-edge shocks (figure 19).

The wing upper-surface wind tunnel data used the same correlation approach as the other upper-surface data; however, the vortex and its influence on heating were allowed to move in position from wind tunnel to flight as the shock interaction was predicted to move. (This amounted to about 10 percent of the wing span.)

The flight test data indicate that this vortex scrubbing is not present under flight conditions between a 30- and 40-deg angle of attack. In fact, the heating appears to be fairly constant outboard of 50-percent semispan, in direct contrast to the wind tunnel data (figure 20).

Inboard of the vortex-influenced region in the wind tunnel (i.e., \leq 60-percent semispan), flight data indicate a similar chordwise trend in heating with that of the wind tunnel. The lowest heating on the wing upper surface consistently exists between 40- and 60-percent chord. This view of the wing upper-surface heating also illustrates the difference between wind tunnel and flight at 60- and 90-percent semispan (figures 21 and 22).

The cause of this greatly reduced heating, especially on the outboard wing upper surface, is not understood at the present time.

Vertical Tail

The vertical tail, as with other areas of the orbiter upper surface, can be divided into regions of nonvortex- and vortex-related flows. The vortex flow appears to be related to the fuselage side vortex based on oil flow data from the wind tunnel (figure 12). Generally, in those areas of nonvortex flow, the flight data and wind tunnel data are in agreement (figure 23). This applies mainly to the lower half of the vertical.

In those regions influenced by vortices, the flow has a pattern similar to the fuselage side. At the low Reynolds numbers, the flow appears to be separated and at a heating level below that of the wind tunnel. As with the fuselage side, flight data show a rapid rise in temperature (heating) at approximately a Reynolds number of 2.0×10^6 . This results in an agreement between flight and wind tunnel data at the higher Reynolds numbers (figure 24).

OMS Pod

The OMS pod has been investigated in terms of flight test data probably more than any other upper surface region to date. This has been due to the critical factor the OMS pod plays in the ability of the orbiter to fly reduced angles of attack from the 40-deg angle of attack development flight test level.

The position of the OMS pod, extending from the orbiter side, makes it extremely susceptible to impingement of flow (vortices) as well as debris traversing along the fuselage side.

The OMS pod receives its peak heating twice during the orbiter's reentry. The upper surface of the pod peaks during the high-alpha portion of entry, while the side of the pod peaks at low angles of attack. Both instances appear to be vortex related. Heating on the side of the pod at a 40-deg angle of attack generally agreed with or was somewhat higher than wind tunnel data (figure 25). However, as the angle of attack decreased, the differences between flight and wind tunnel increased for the side of the pod.

The impinging vortex transforms the flow on the pod from separated to attached. First, the flow impinges at about 20 percent of the pod length. Then, as the angle of attack decreases or the Reynolds number increases, the attachment point moves forward. Once the flow becomes attached, changes in the major heating parameters have little influence on heating, based on wind tunnel data. However, in the transition phase between separation and attached flow, heating is extremely sensitive to small variations in angle of attack, yaw, and Reynolds number. Under flight conditions, it appears that the flow becomes attached at a higher angle of attack and at a lower Reynolds number than under wind tunnel conditions.

This sensitivity to angle of attack and flow attachment occurring earlier in flight was made evident based on data from several pitch maneuvers [push over/pull up (POPU)]. These maneuvers were planned to expose the orbiter to more severe angles of attack (lower) for short periods of time, thereby obtaining heat transfer data while not exposing the structure to any excessive heat loads. These transient maneuvers were performed at discrete velocities on STS-2 (21,000 ft/sec), STS-4 (12,000 ft/sec and 8,400 ft/sec), and STS-5 (18,000 ft/sec). The POPU maneuver was performed by varying the angle of attack by approximately 1 deg/sec from the nominal to the minimum, from the minimum to the maximum, and then back to the nominal angle of attack. Dwell time at the angle of attack extremes varies from 1 to 2 sec to almost 10 sec. This data, though only at the minimal angle of attack for less than 10 sec, indicated higher temperatures in flight than in the wind tunnel (figures 25b and 25c).

The element of uncertainty still in the POPU data is in determining the steady-state surface temperature (heating rate) from a thermocouple below the outer mold line (OML) experiencing only a few seconds of increased heating. The possible variation due to this uncertainty is shown in figures 26 and 27. This uncertainty relates not only to surface temperatures but to the total heat load influencing the structure temperature and thus to predictions of orbiter capability.

CONCLUDING REMARKS

The orbiter entry heating lessons learned from the development flight test program are significant, with many yet to be discovered. This development test program has provided quality entry aerothermodynamic data as a basis for these discoveries. These data, although still in the preliminary analysis phases, support the use of wind tunnel test data for the design of TPS's for hypersonic reentry vehicles and will allow more optimized TPS's for future vehicles. The design of these future vehicles will be further enhanced by both utilizing and developing analytical solutions derived from Navier-Stokes equations, thereby greatly reducing parametric design efforts and scaling-to-flight difficulties experienced with wind tunnel data.

REFERENCES

1. Harthun, M. H.; Blumer, C. B.; and Miller, B. A.: Orbiter Windward Surface Entry Heating--Post-Orbital Flight Test Program Update. Shuttle Performance: Lessons Learned, NASA CP-2283, Part 2, 1983, pp. 781-805.
2. Cunningham, J. A. and Haney, J. W.: Space Shuttle Wing Leading Edge Heating Environment Prediction Derived From Development Flight Data. Shuttle Performance: Lessons Learned, NASA CP-2283, Part 2, 1983, pp. 1083-1110.
3. An Investigation of Entry Heating on the 0.0175-Scale Space Shuttle Orbiter (Model 60-0) in the AEDC UKV Tunnel 'B'. NASA CR-160490, Vols 1-4, July 1980.
4. Results of Heat Transfer Tests on a 0.0175-Scale Space Shuttle Orbiter Model (56-0) in the AEDC VKF 'B' Hypersonic Wind Tunnel. NASA CR-144596, Mar. 1976.
5. Results of Heat Transfer Test in the Arnold Engineering Development Center - Von Karman Facility Tunnels A and B Utilizing Space Shuttle Orbiter Thin Skin Thermocouple Models 56-0, 60-0, and 83-0 Tests: OH 84B, OH 105, IH 102. NASA CR-160828, Vols 1-6, Aug. 1981.
6. Test Results From the NASA/Rockwell International Space Shuttle 0.0175-Scale Orbiter Models 56-0/60-0 and 0.04-Scale Orbiter Forebody Model 83-0 Conducted in the AEDC/VKF-B 50-Inch Hypersonic Wind Tunnel. NASA CR-167349, Vols 1-3, July 1982.
7. NASA/RI OH-111 Orbiter Abort Heating Test. NASA CR-167380, Vols 1-5, Sept. 1981.
8. Test Results From the NASA/Rockwell International Space Shuttle 0.0175-Scale Orbiter Models 56-0/60-0 and 0.04-Scale Orbiter Forebody Model 83-0 Conducted in the NASA/ARC 3.5-Foot Hypersonic Wind Tunnel. NASA CR-160844, Oct. 1981.
9. Results of Test on a 0.0175-Scale Model (60-0) of the Space Shuttle Orbiter to Determine Reentry Mode Convective Heat Transfer Rates on the Upper Wing Surface and SSME Nozzles in the AEDC VKF 'B' Hypersonic Wind Tunnel (OH98). NASA CR-160501, Vols 1 and 2, Sept. 1980.
10. Space Shuttle Orbital Maneuvering System Pod Heating Test at Mach Number 8. AEDC-TSR-80-V2, Jan. 1980.

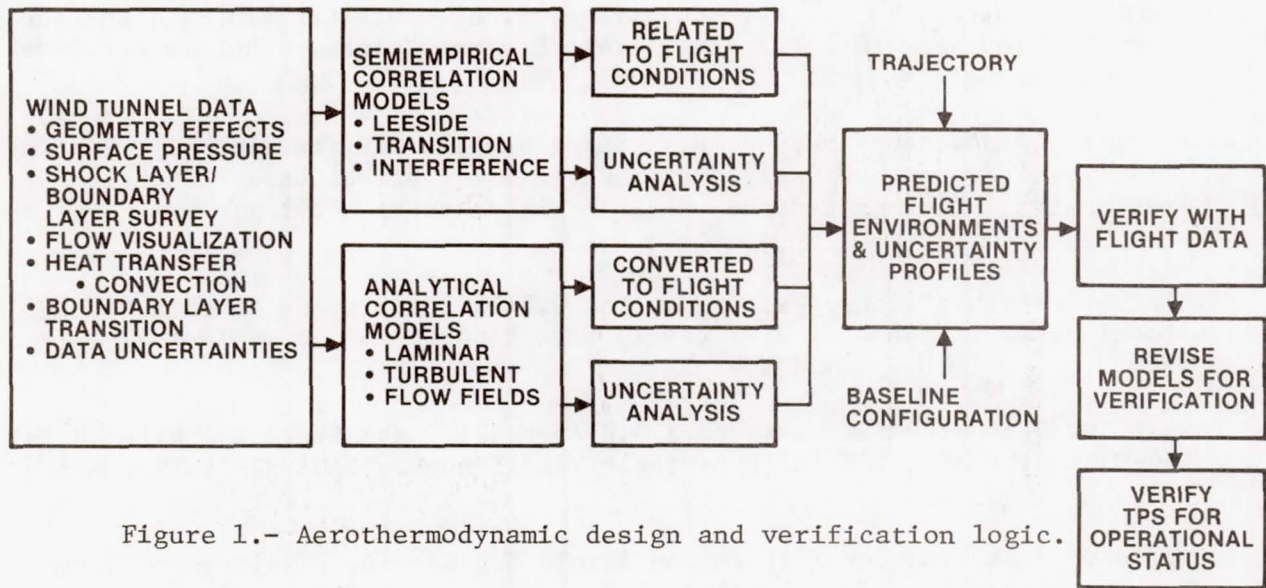


Figure 1.- Aerothermodynamic design and verification logic.

- 50 WIND TUNNEL TEST
- 5,250 HOURS
- ~ 9 CONFIGURATIONS (07D-ATP, 089, 089B-MOD, 130 MOD, 139, 139 MOD, 140B, 147B, 140C-STS-1)
- 7 FACILITIES: NASA LRC/VDT, NASA LRC/CF4, NASA LRC/CFHT, NASA AMES 3.5 FT, CALSPAN, AEDC-B, AEDC-F
- 10 MODEL SCALES: 0.006, 0.01, 0.014, 0.0175, 0.025, 0.04, 0.08, 0.1, 0.111, FULL
- 6 TYPES OF INSTRUMENTATION: THERMOCOUPLE, CALORIMETER, THIN FILM GAGE, PAINT, PRESSURE TAP, INFRARED
- 4 TYPES OF DATA: TEMPERATURE, HEATING RATE, PRESSURE, BOUNDARY LAYER PROBES
- MACH NUMBERS: 5.3 → 19
- R_E/FT $0.5 \times 10^6 \rightarrow 9.0 \times 10^6$
- α $0^\circ \rightarrow 50^\circ$
- β $0^\circ \pm 0.5^\circ, \pm 1^\circ, \pm 2^\circ, + 5^\circ + 10^\circ$
- δ_E -30° TO $+ 10^\circ$
- δ_{BF} $0^\circ, 5^\circ, 10^\circ, 15^\circ, 22^\circ$

Figure 2.- Wind tunnel data base.

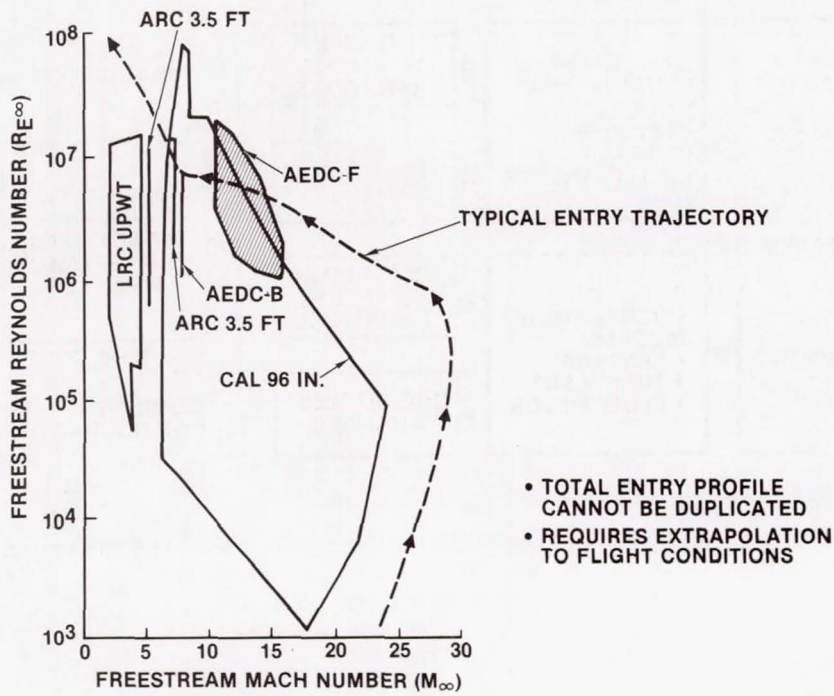


Figure 3.- Wind tunnel test simulation.

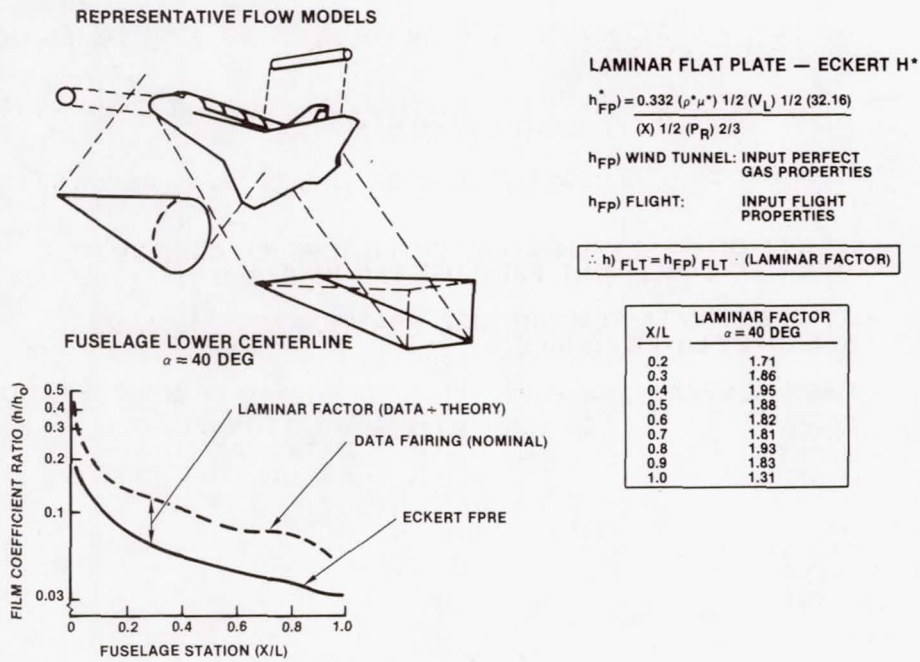


Figure 4.- Orbiter lower-surface methodology; slender body approach.

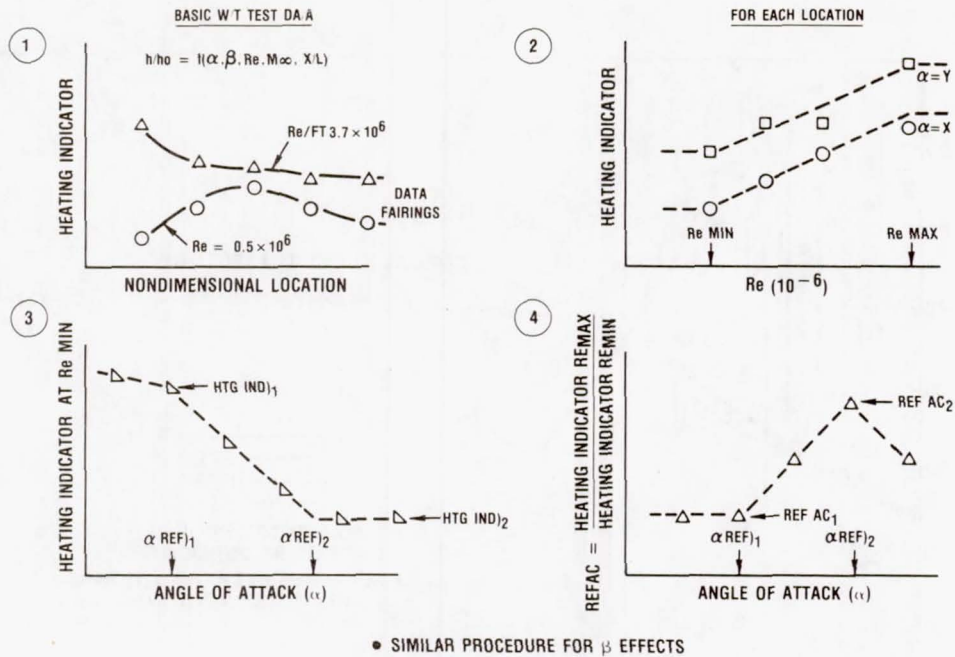


Figure 5.- Orbiter upper-surface methodology.

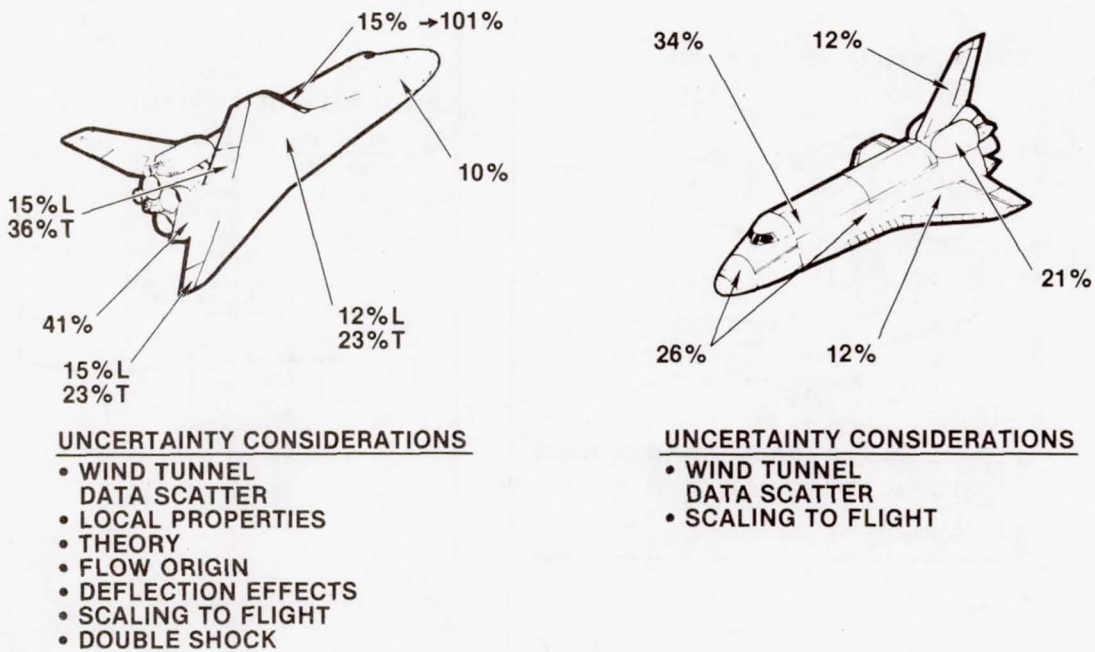


Figure 6.- Heating uncertainties for STS-1.

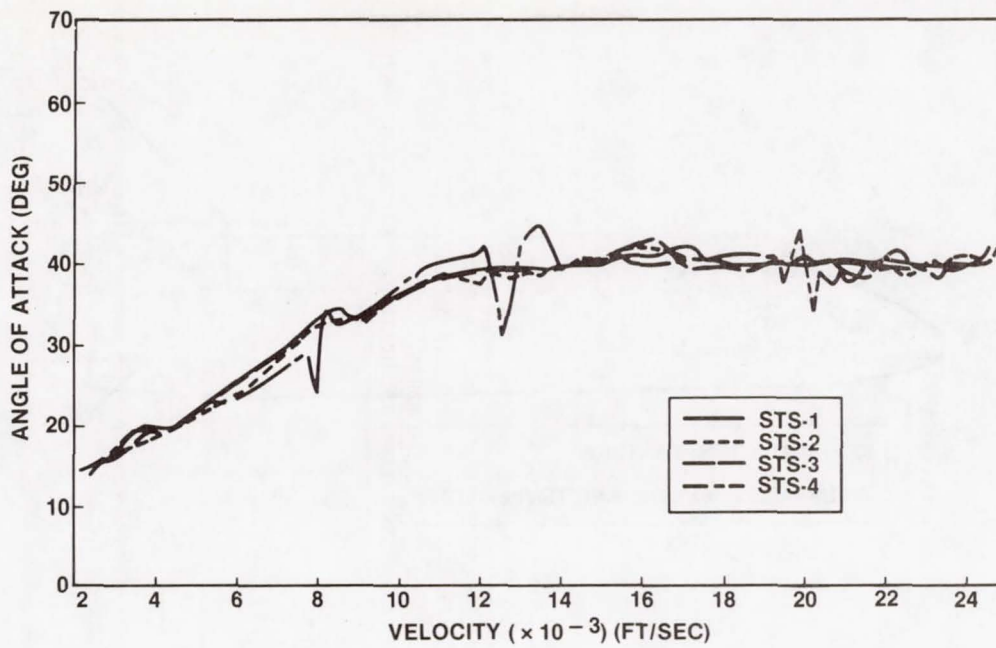
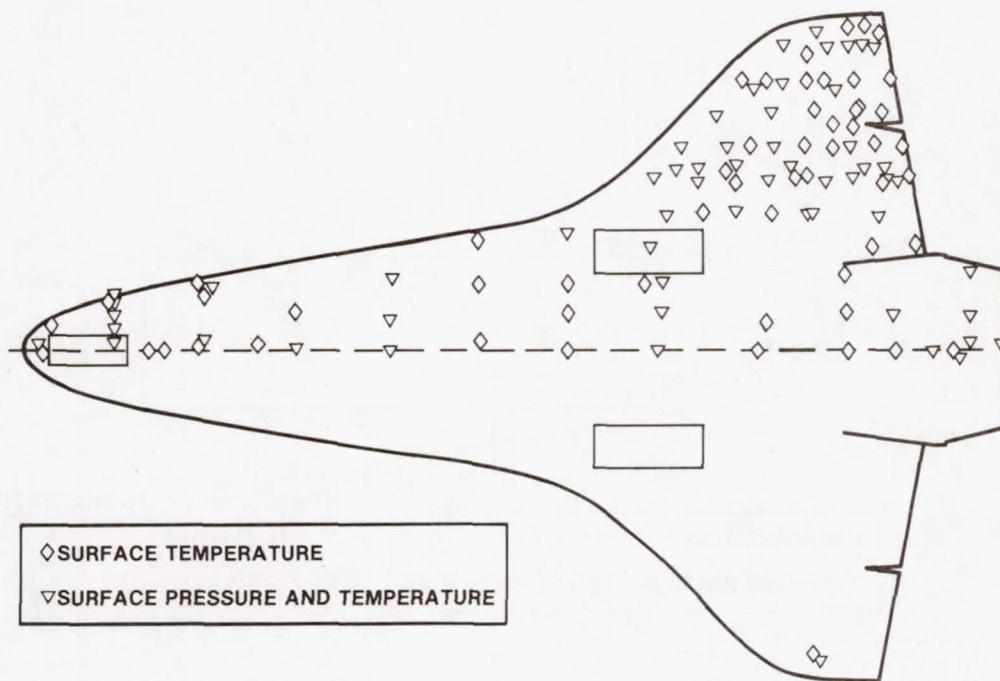
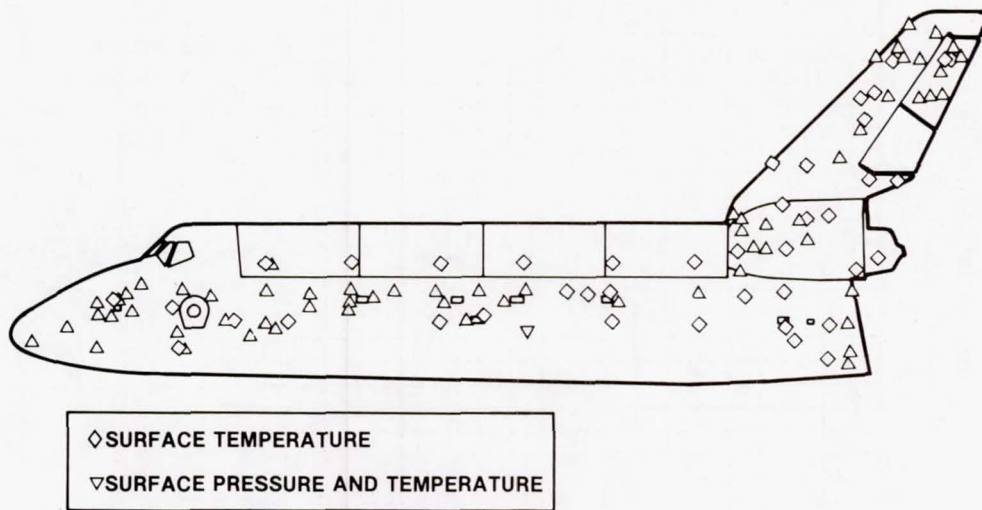


Figure 7.- Orbital flight test angle-of-attack experience.

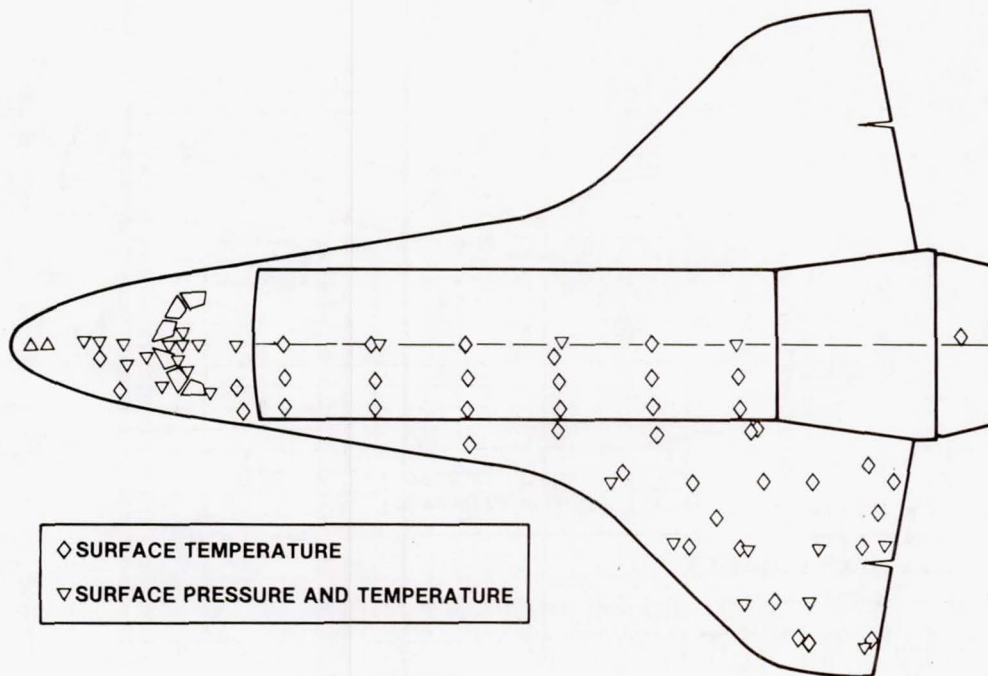


(a) Lower surface.

Figure 8.- Aerothermodynamic instrumentation locations.

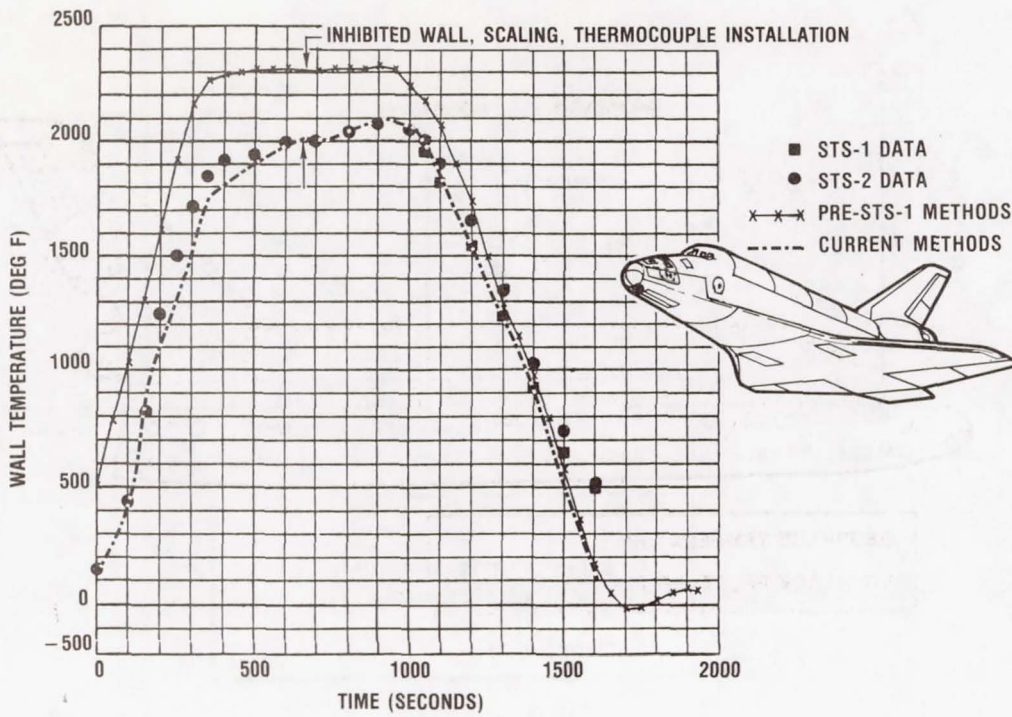


(b) Side surface.

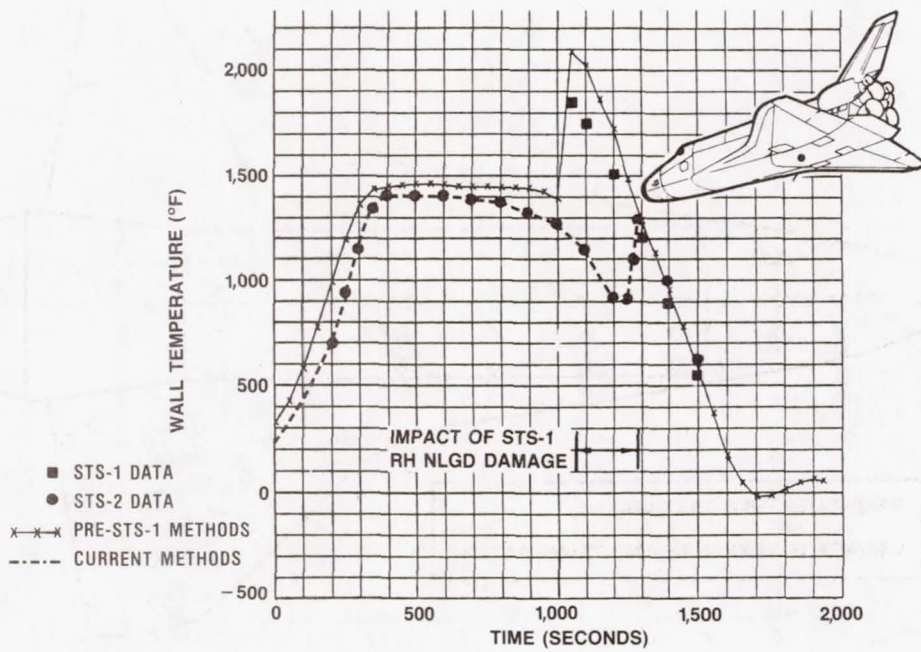


(c) Upper surface.

Figure 8.- Concluded.



(a) Centerline - (X_0 268) ($X/L = 0.025$).



(b) Centerline - (X_0 1,128.0) ($X/L = 0.70$).

Figure 9.- Fuselage lower surface.

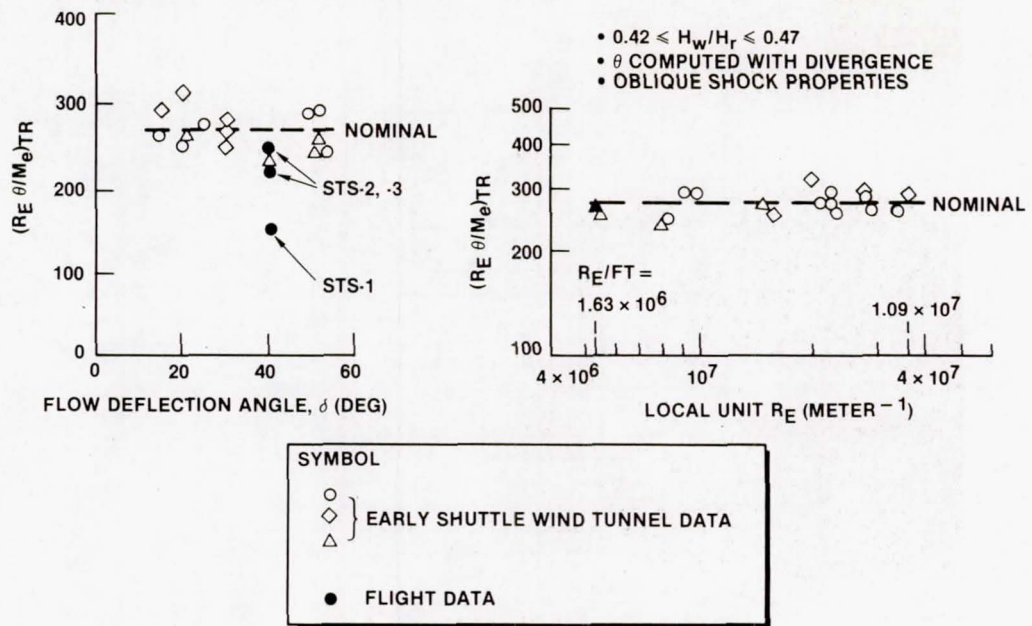


Figure 10.- Delta wing orbiter boundary layer transition correlation.

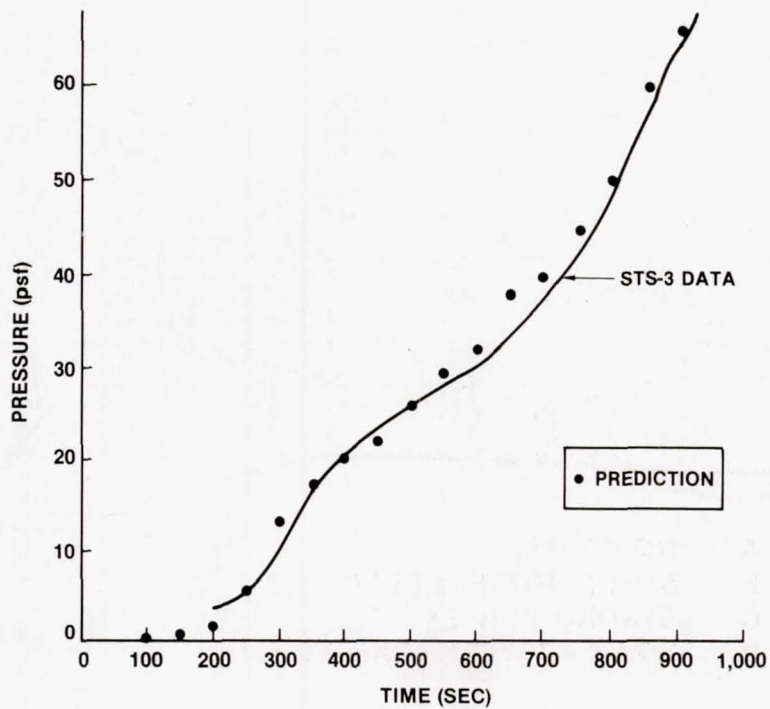
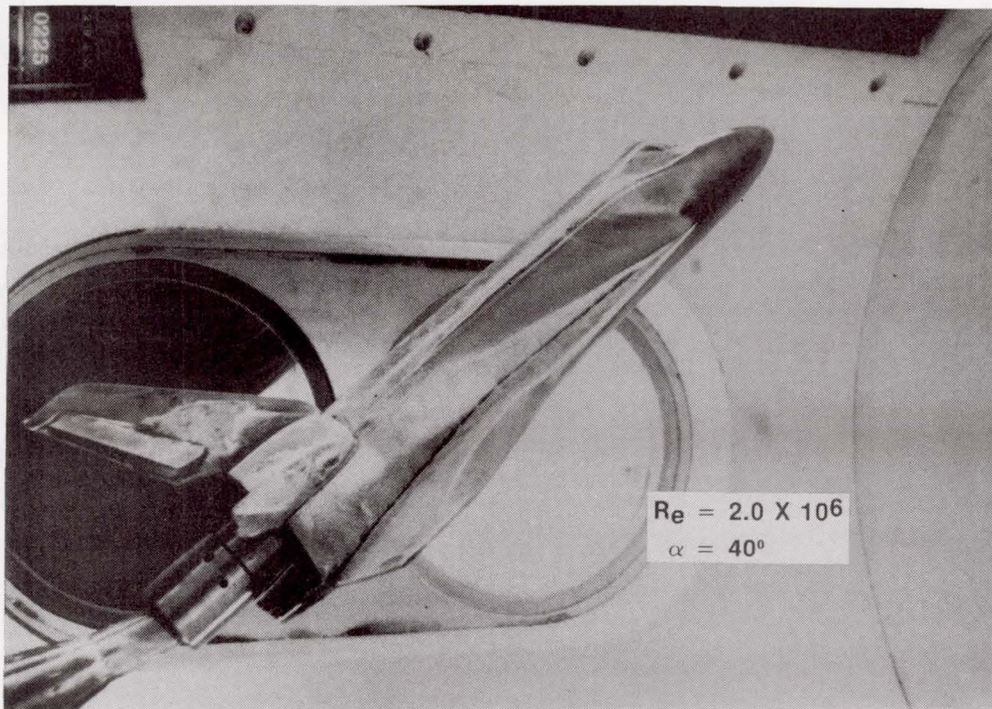
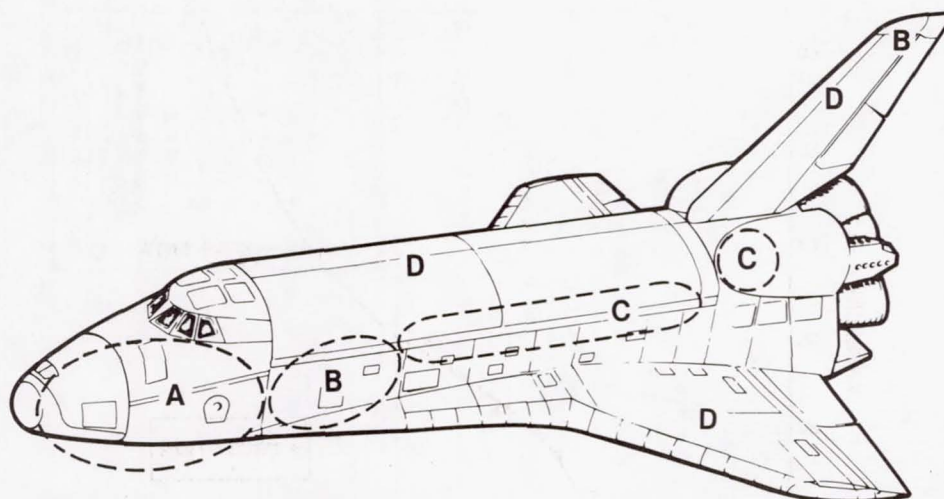


Figure 11.- STS-3 postflight lower centerline - $X/L = 0.40$ (V07P9472).



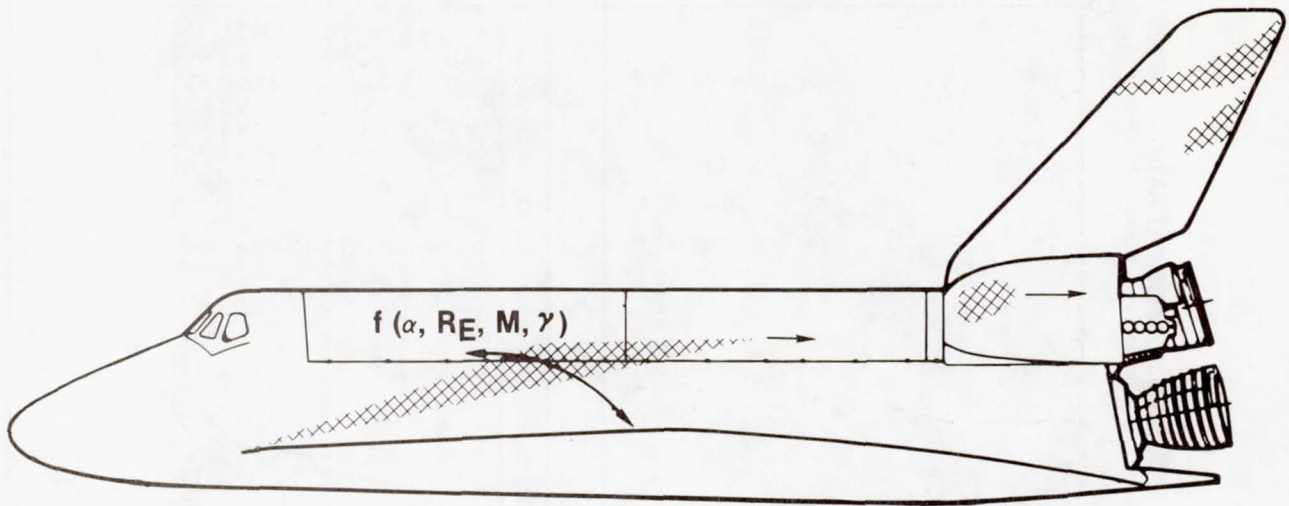
(a) Oil flow patterns in wind tunnel. $\alpha = 40^\circ$.



- | | |
|---------------|-------------------------------|
| ZONE A | NO VORTEX |
| ZONE B | SLIGHT/MODERATE VORTEX |
| ZONE C | STRONG VORTEX |
| ZONE D | WEAK VORTEX/SEPARATED |

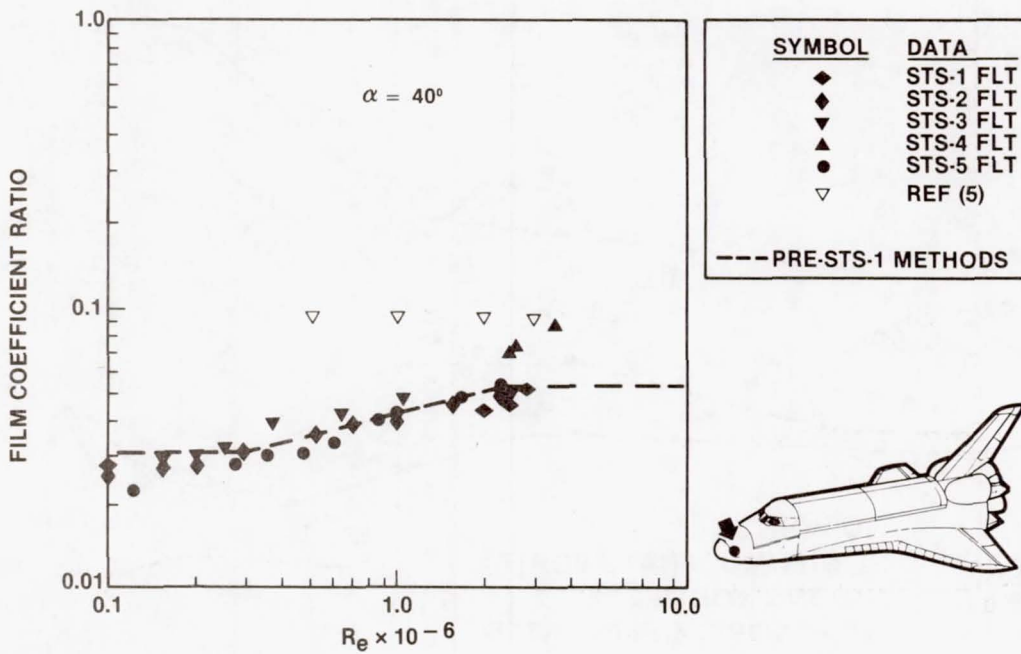
(b) Leeward side vortex flows.

Figure 12.- Fuselage side heating patterns.



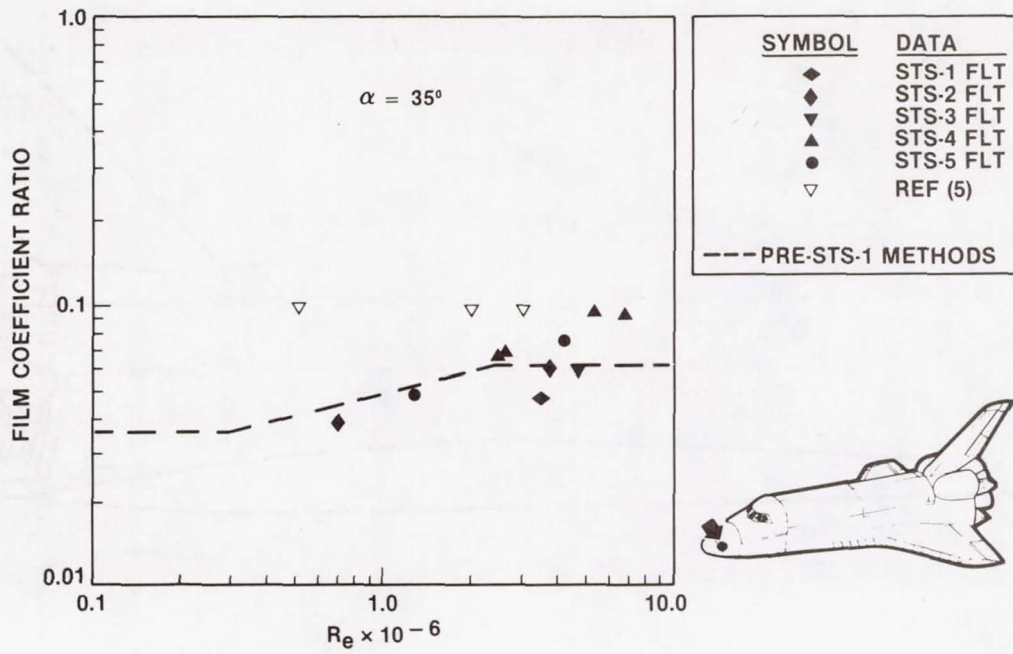
(c) Vortex scrubbing.

Figure 12.- Concluded.

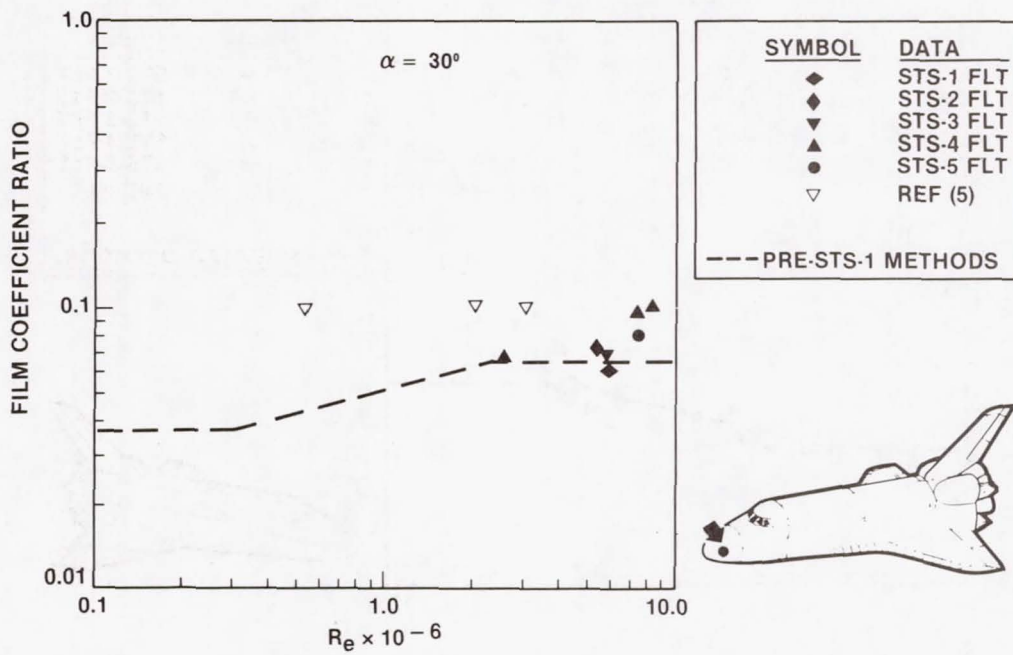


(a) $\alpha = 40^\circ$.

Figure 13.- Fuselage side heating correlation at location V07T9880.

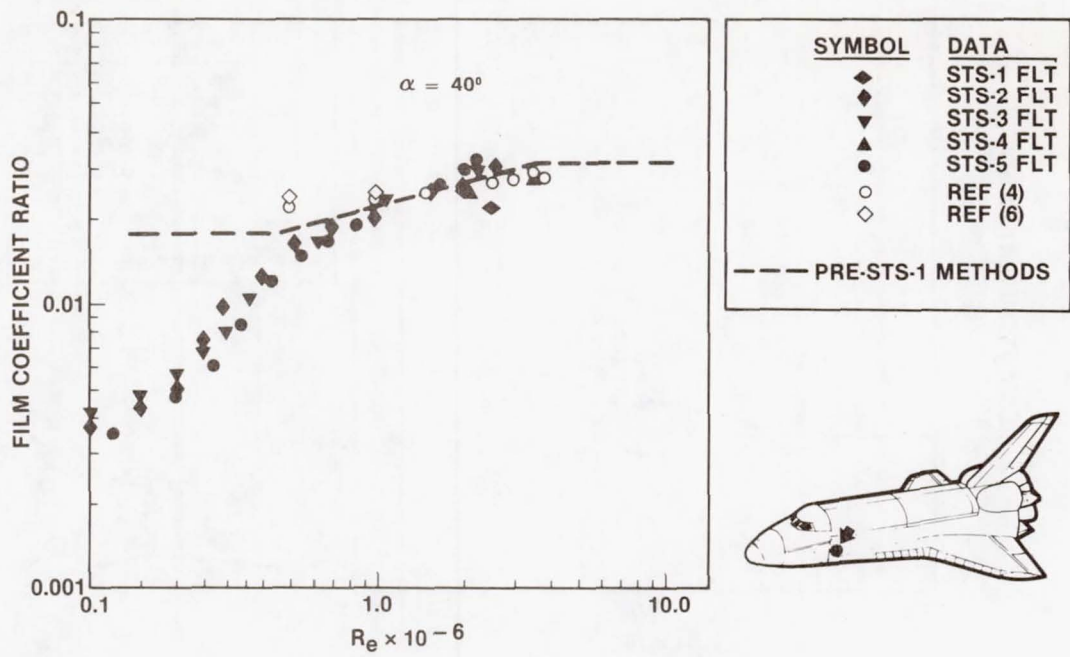


(b) $\alpha = 35^\circ$.

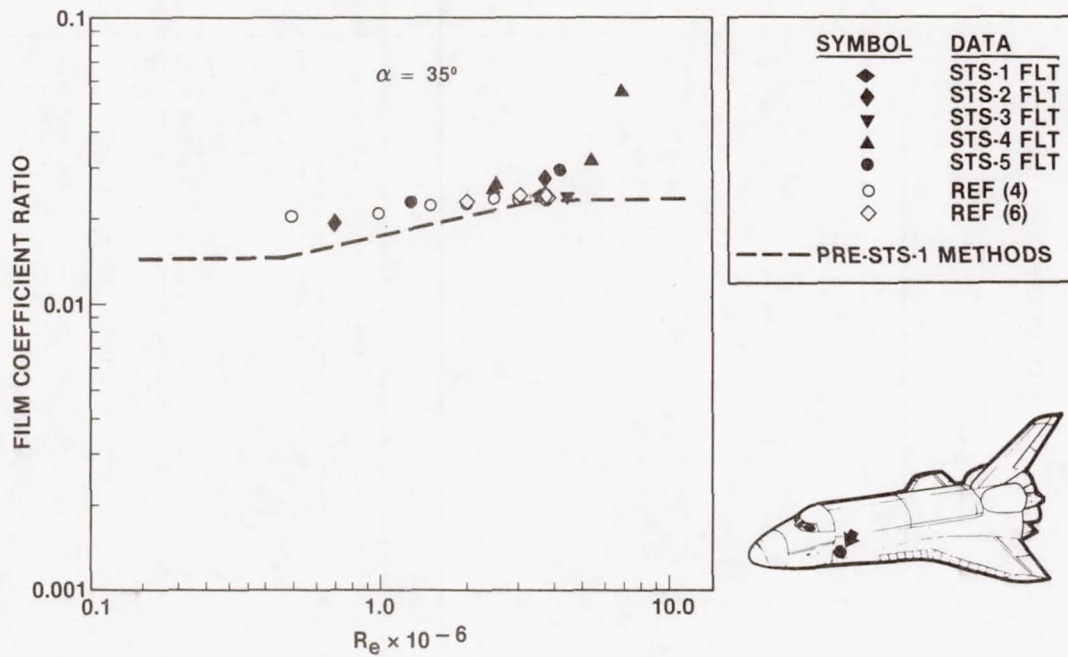


(c) $\alpha = 30^\circ$.

Figure 13.- Concluded.

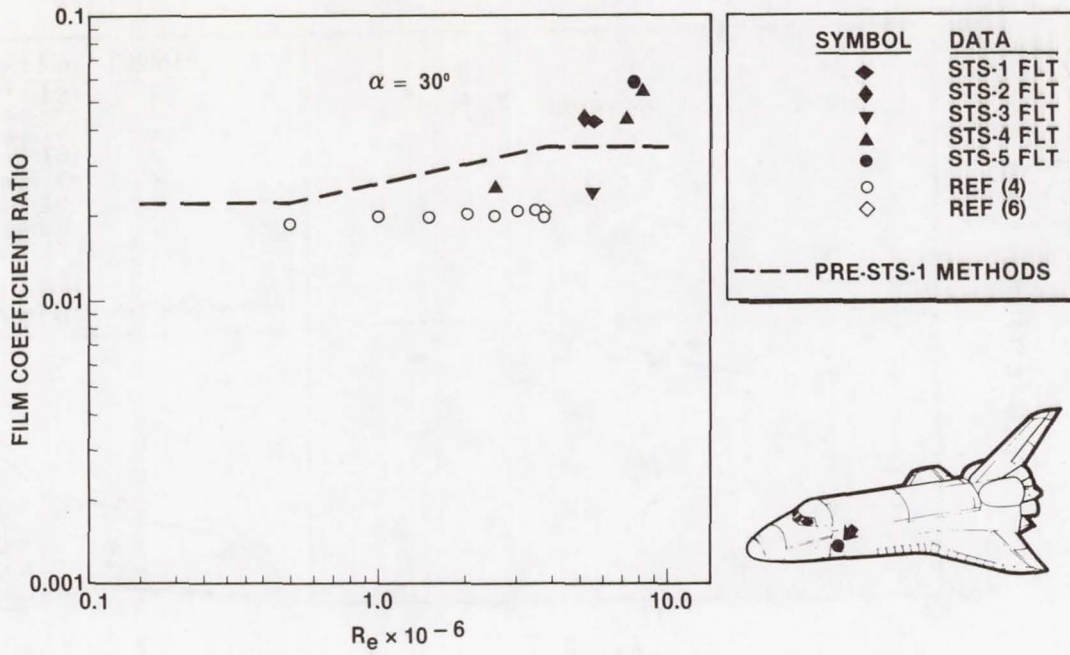


(a) $\alpha = 40^\circ$.



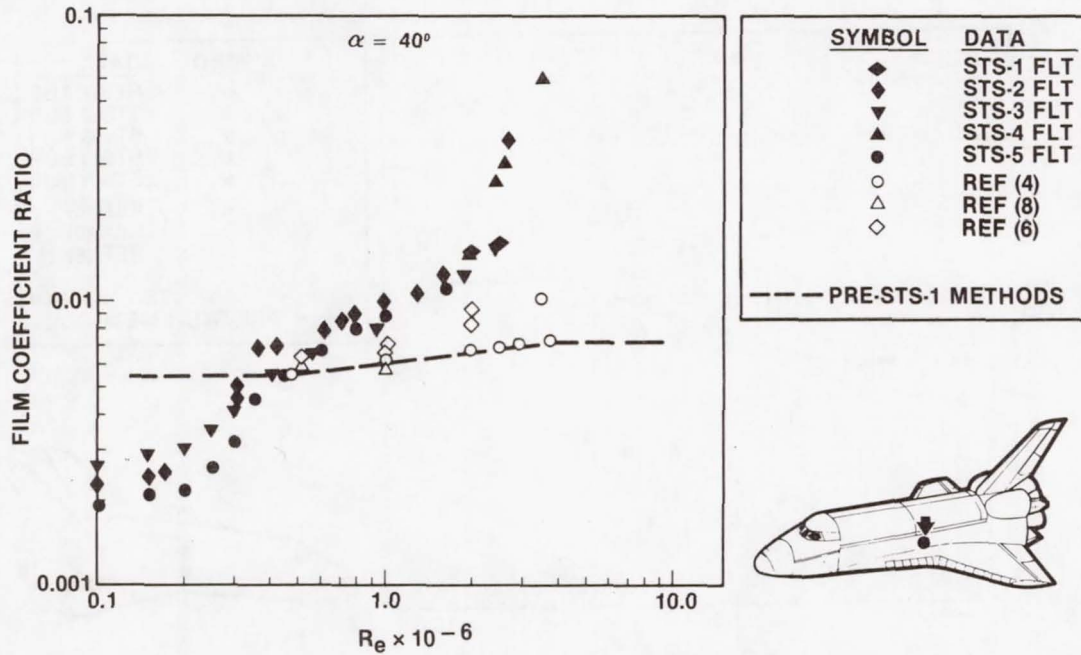
(b) $\alpha = 35^\circ$.

Figure 14.- Fuselage side heating correlation at location V07T9859.



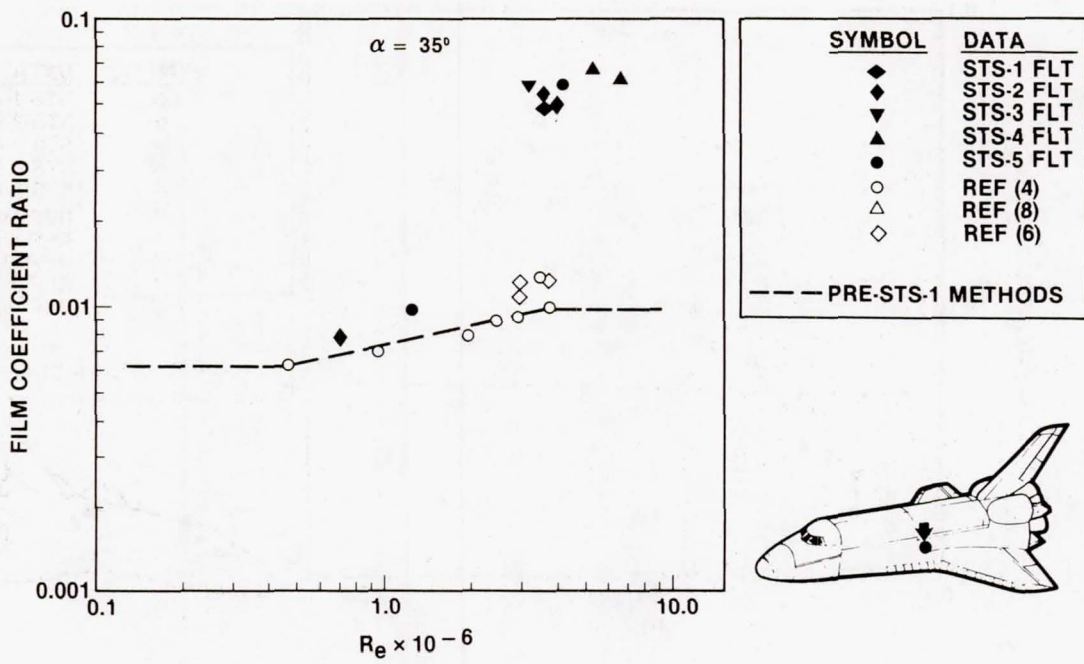
(c) $\alpha = 30^\circ$.

Figure 14.- Concluded.

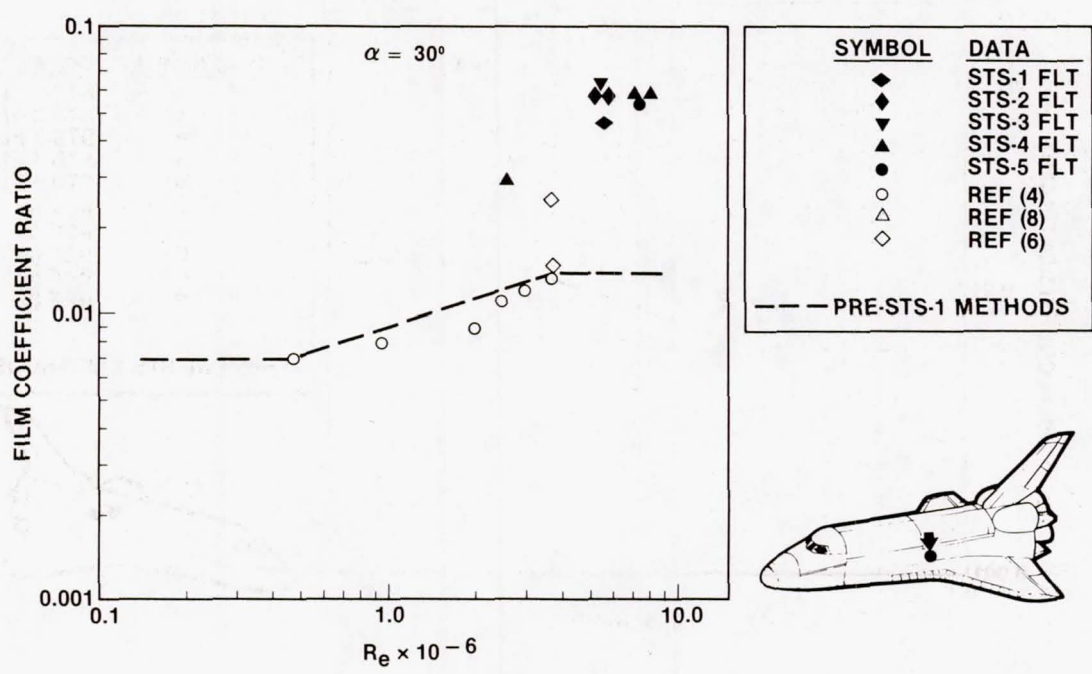


(a) $\alpha = 40^\circ$.

Figure 15.- Fuselage side heating correlation at location V07T9905.

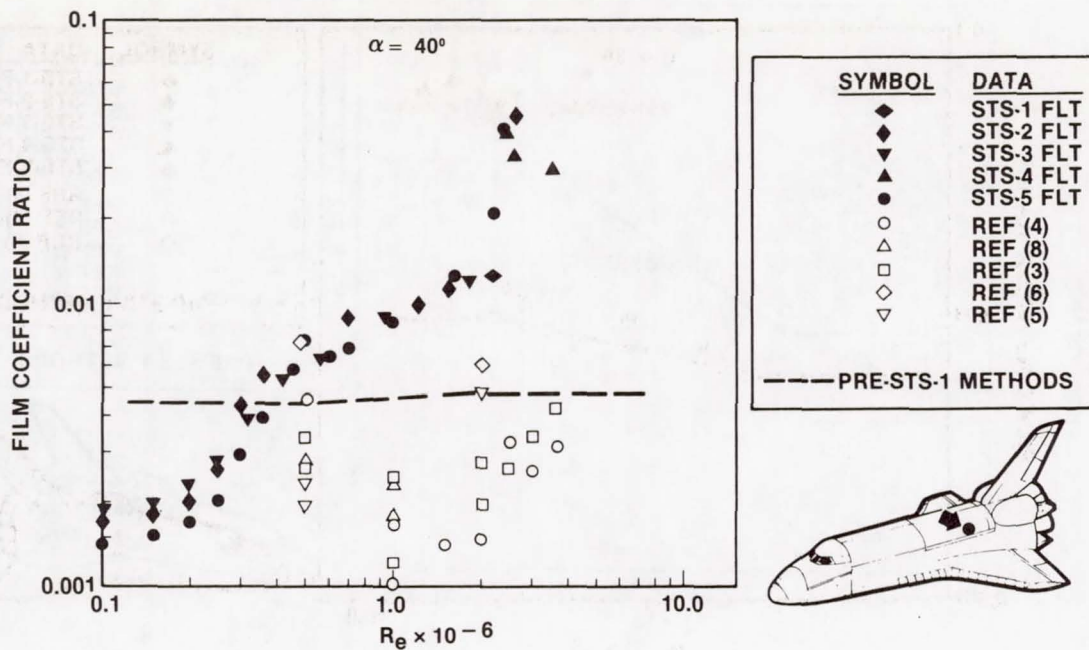


(b) $\alpha = 35^\circ$.

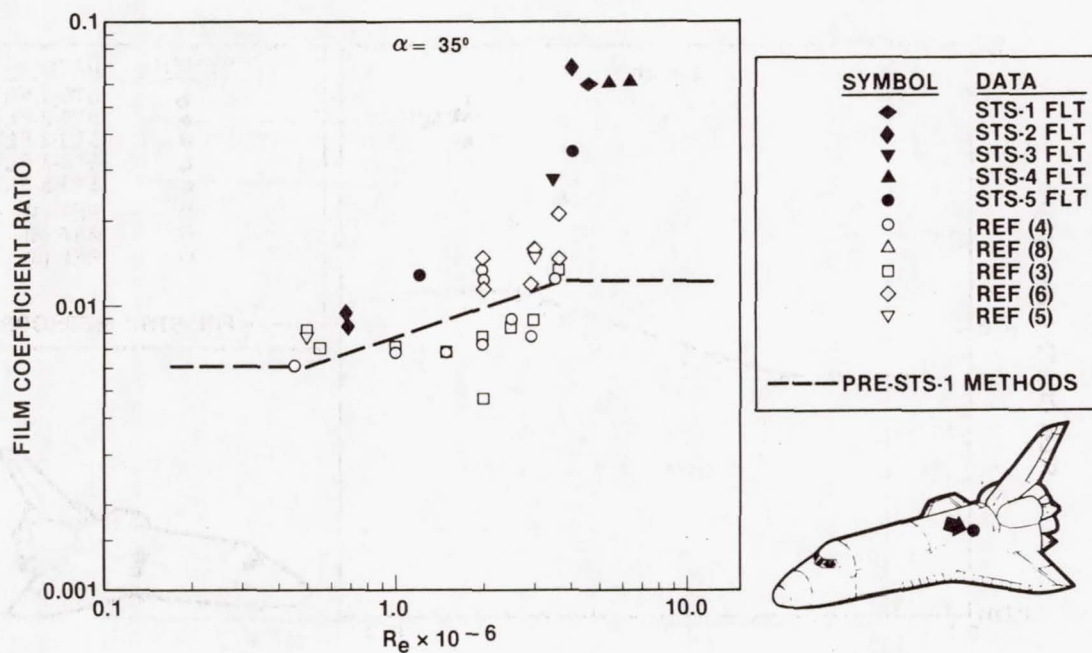


(c) $\alpha = 30^\circ$.

Figure 15.- Concluded.

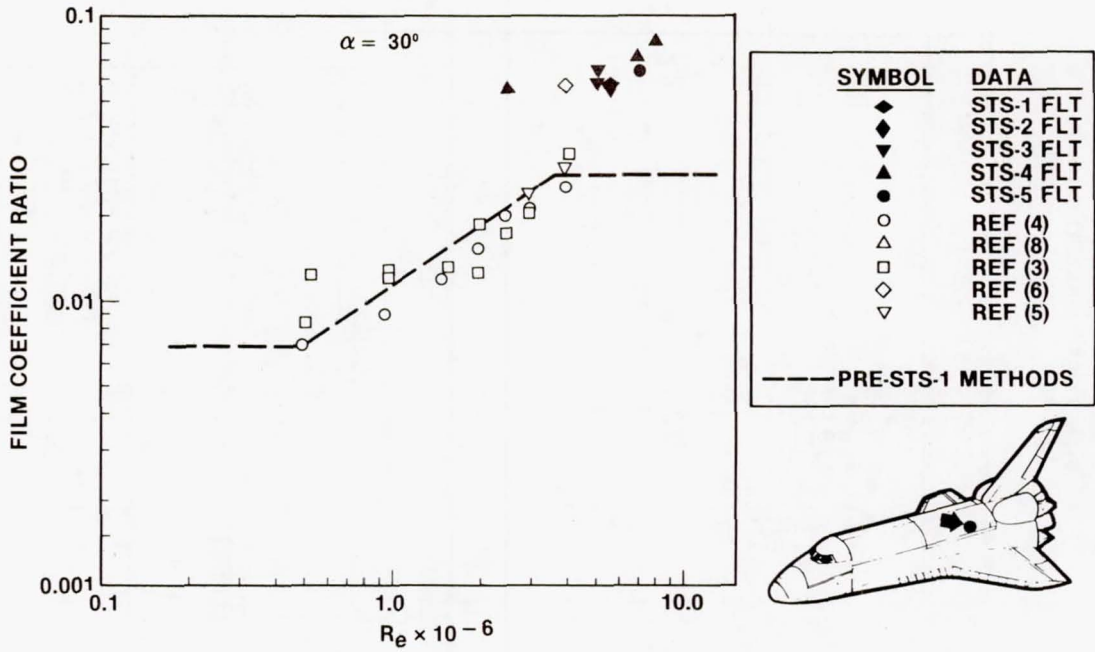


(a) $\alpha = 40$



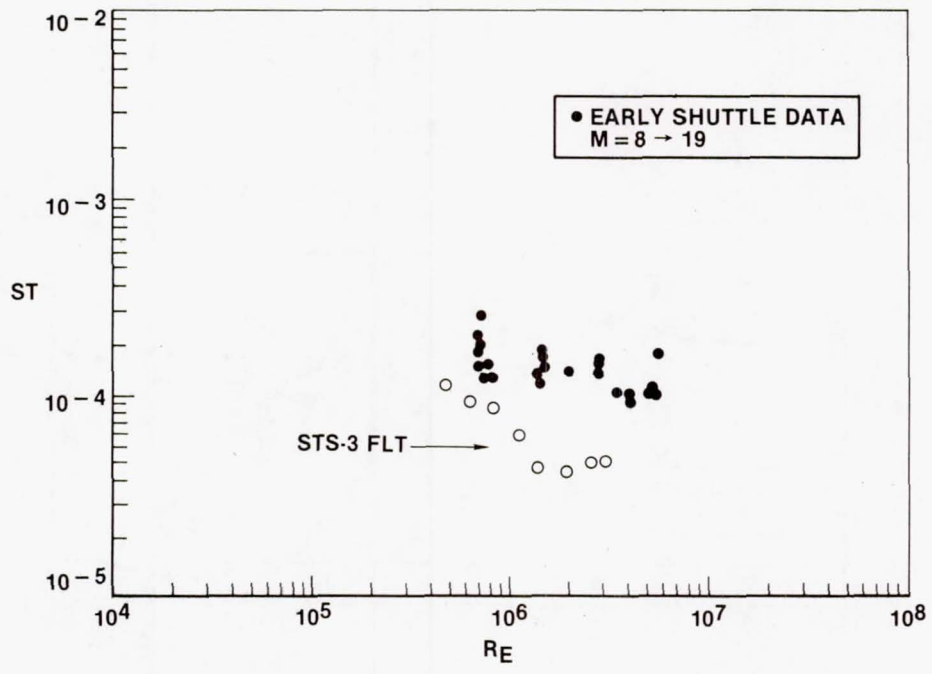
(b) $\alpha = 35^\circ$

Figure 16.- Fuselage side heating correlation at location V07T9925.



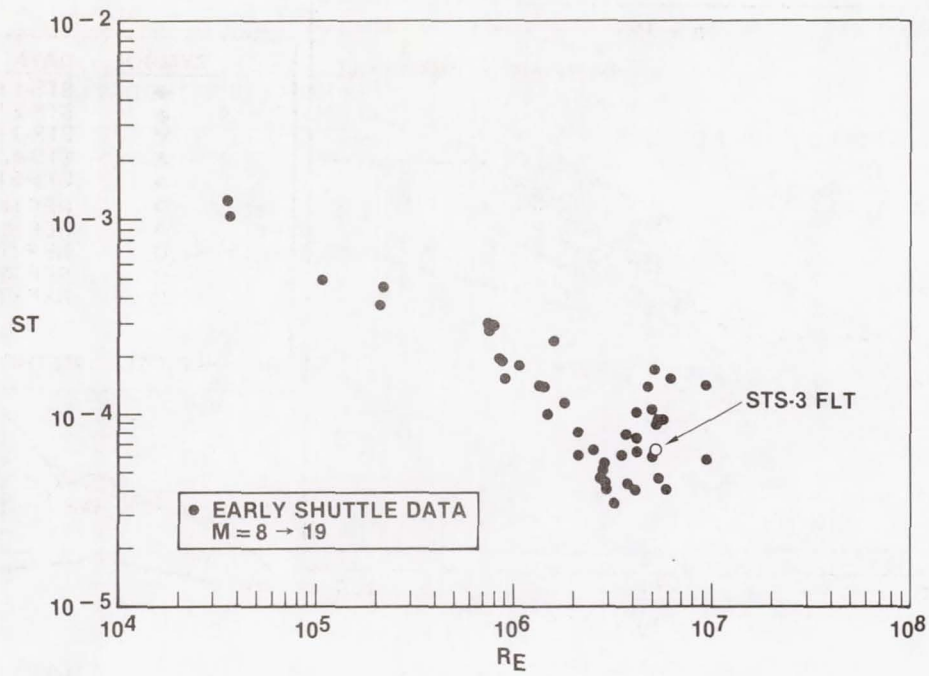
(c) $\alpha = 30^\circ$.

Figure 16.- Concluded.

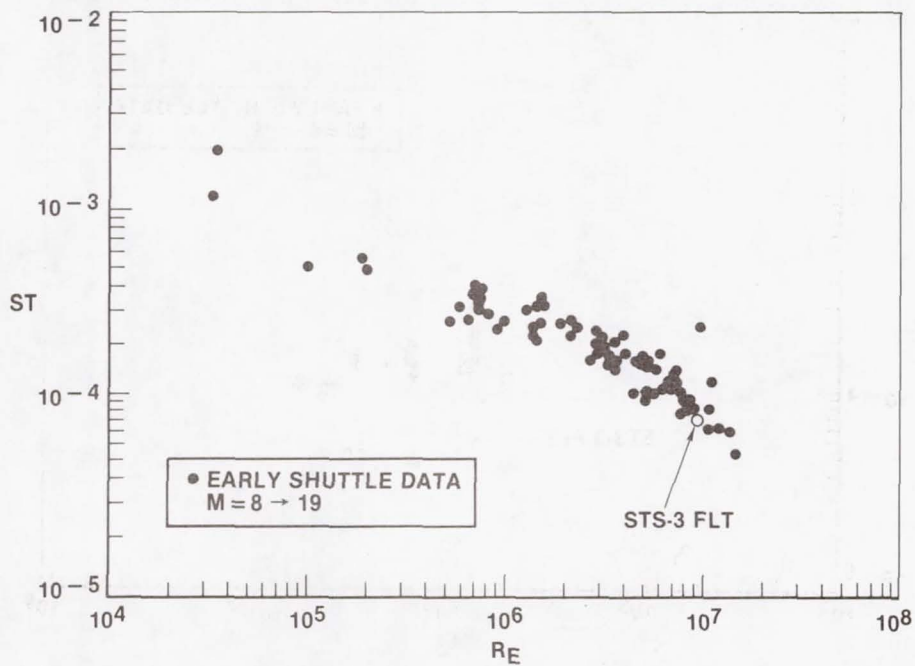


(a) $\phi = 180^\circ$, $\alpha = 40^\circ$, $X/L = 0.7$.

Figure 17.- Fuselage upper surface.



(b) $\phi = 180^\circ$, $\alpha = 35^\circ$, $X/L = 0.7$.



(c) $\phi = 180^\circ$, $\alpha = 30^\circ$, $X/L = 0.7$.

Figure 17.- Concluded.

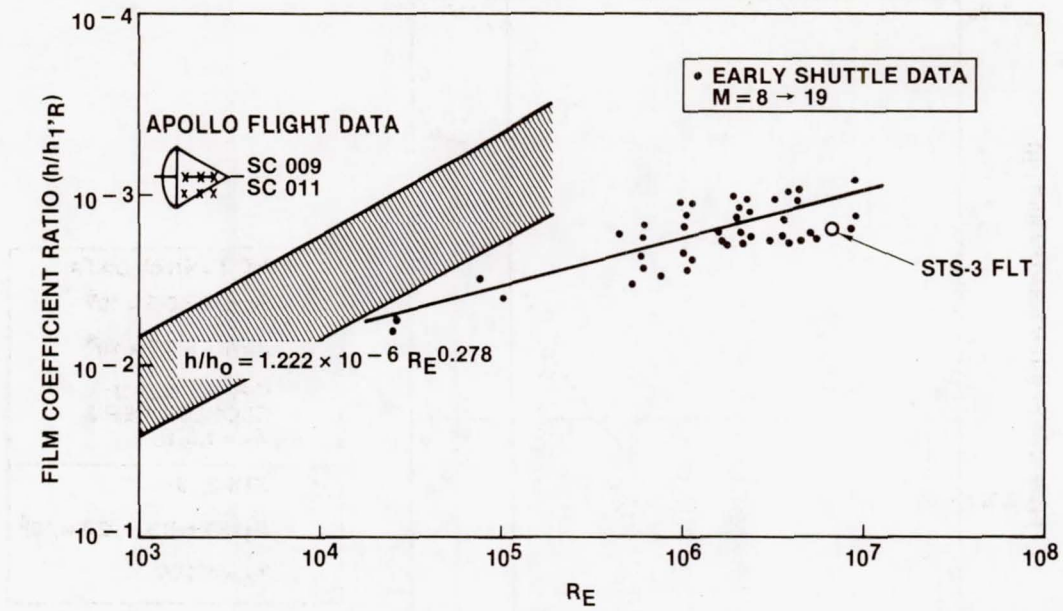


Figure 18.- Flight data versus wind tunnel. Fuselage upper centerline - $X/L = 0.5$, $\alpha = 30^\circ$.

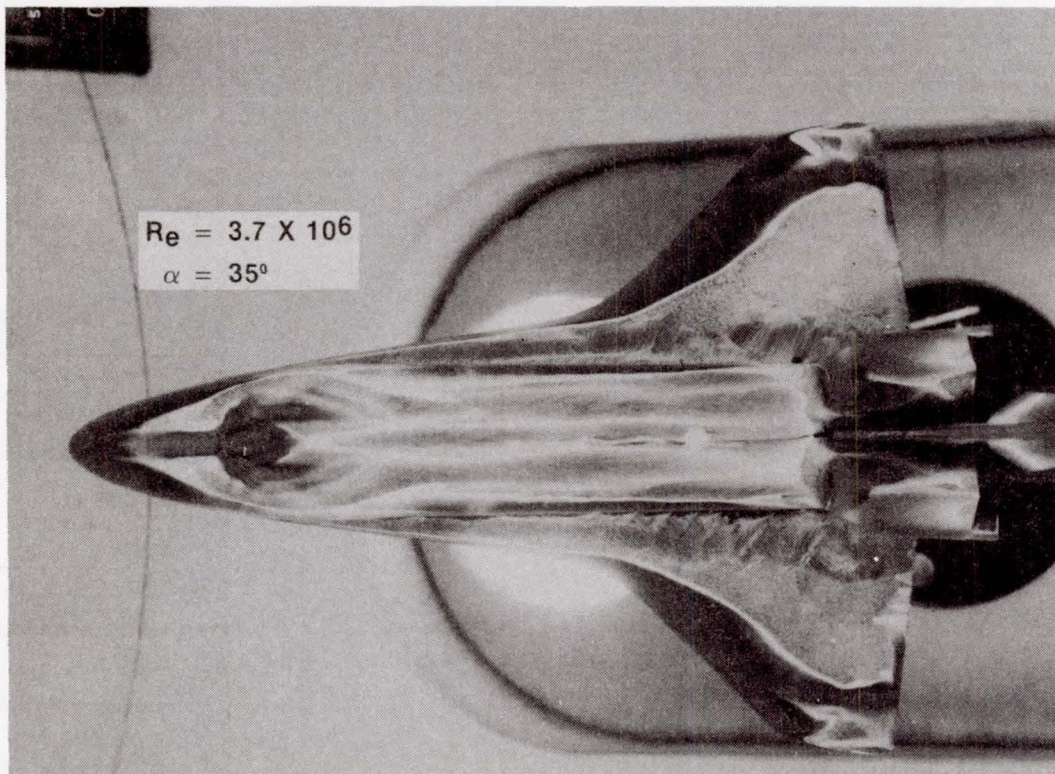


Figure 19.- Oil flow patterns in wind tunnel. $\alpha = 35^\circ$.

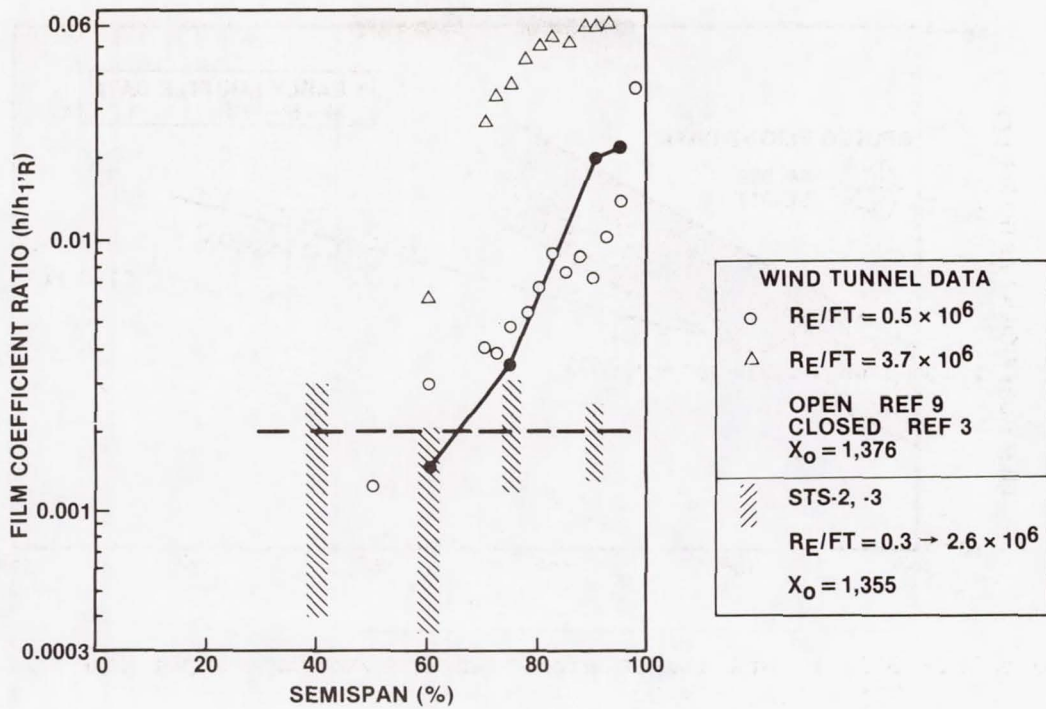


Figure 20.- Wing upper surface - spanwise variation.

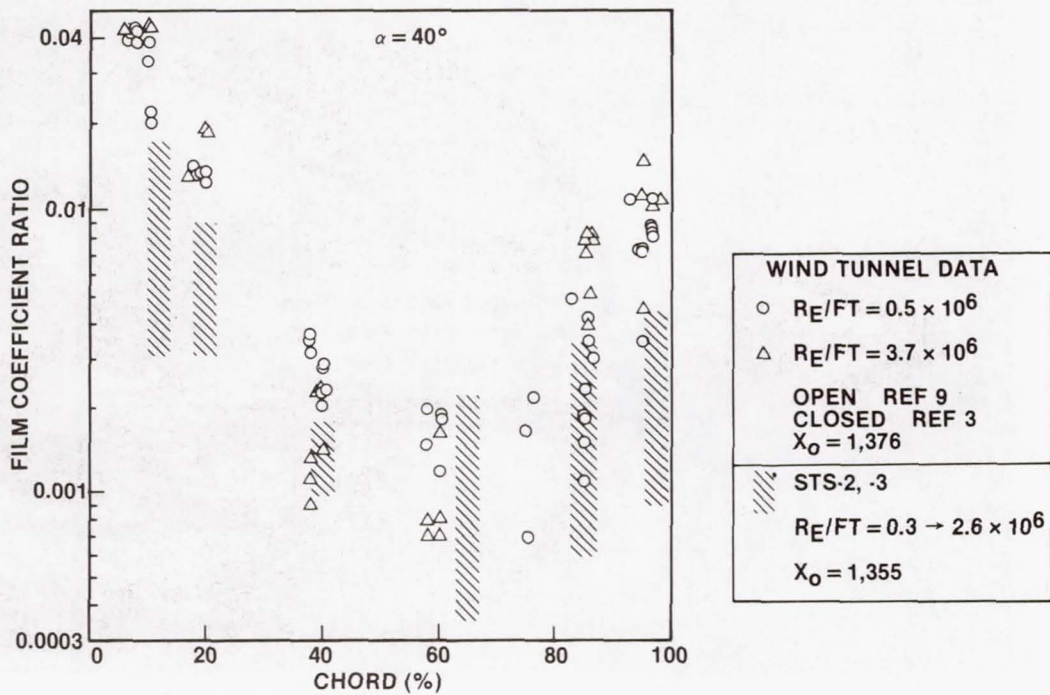


Figure 21.- Wing upper surface - 60-percent semispan.

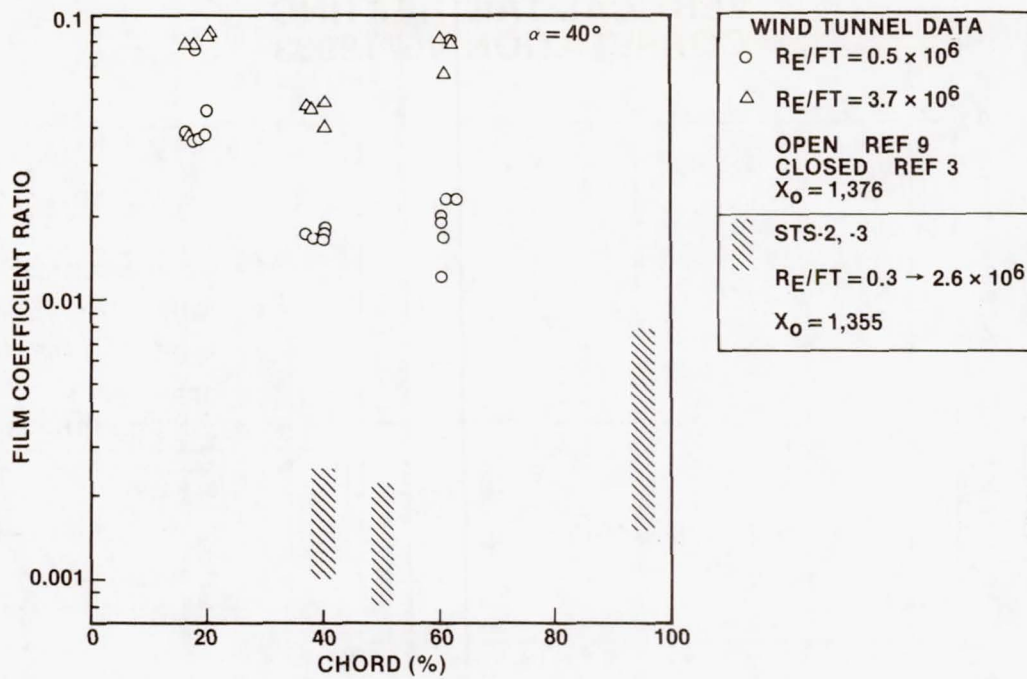
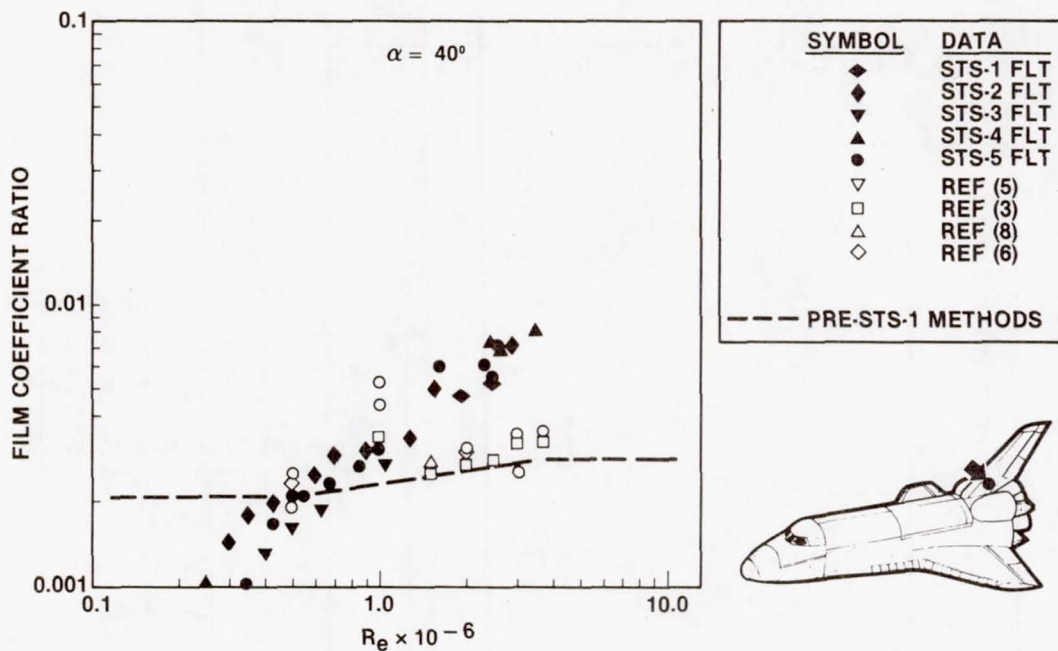


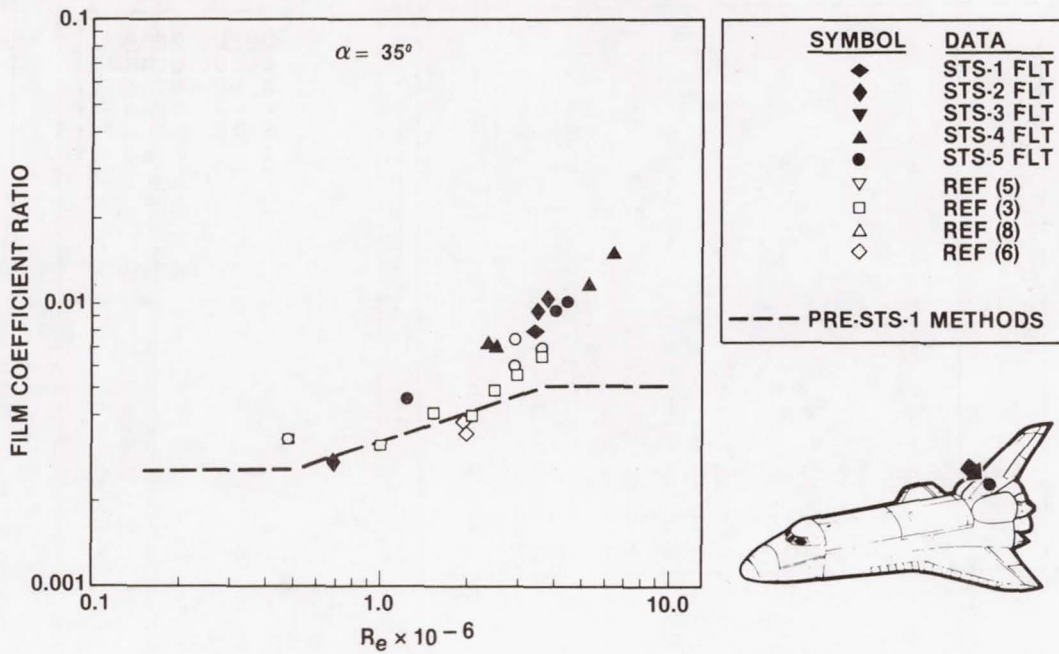
Figure 22.- Wing upper surface - 90-percent semispan.



(a) $\alpha = 40^\circ$.

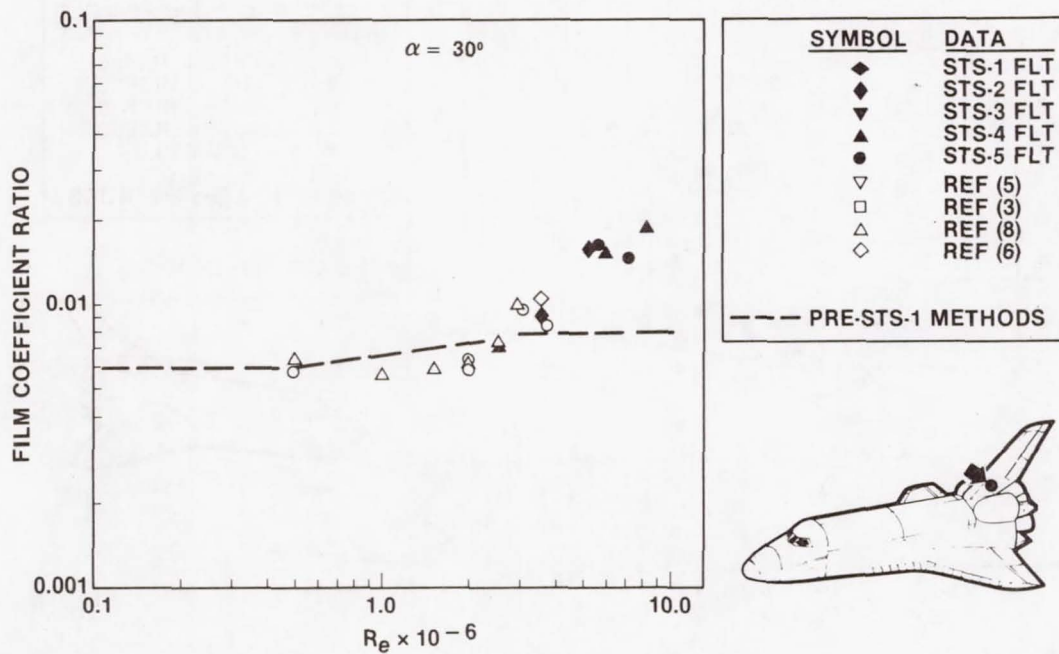
Figure 23.- Vertical tail heating correlation.

VERTICAL TAIL HEATING CORRELATION V07T9933



(b) $\alpha = 35^\circ$.

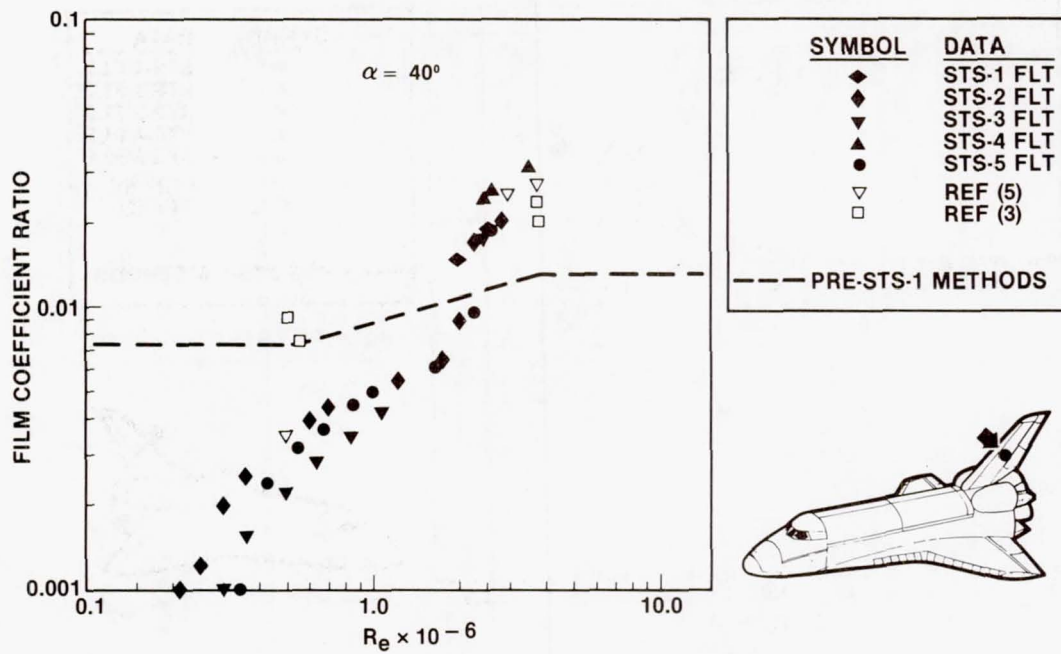
VERTICAL TAIL HEATING CORRELATION V07T9933



(c) $\alpha = 30^\circ$.

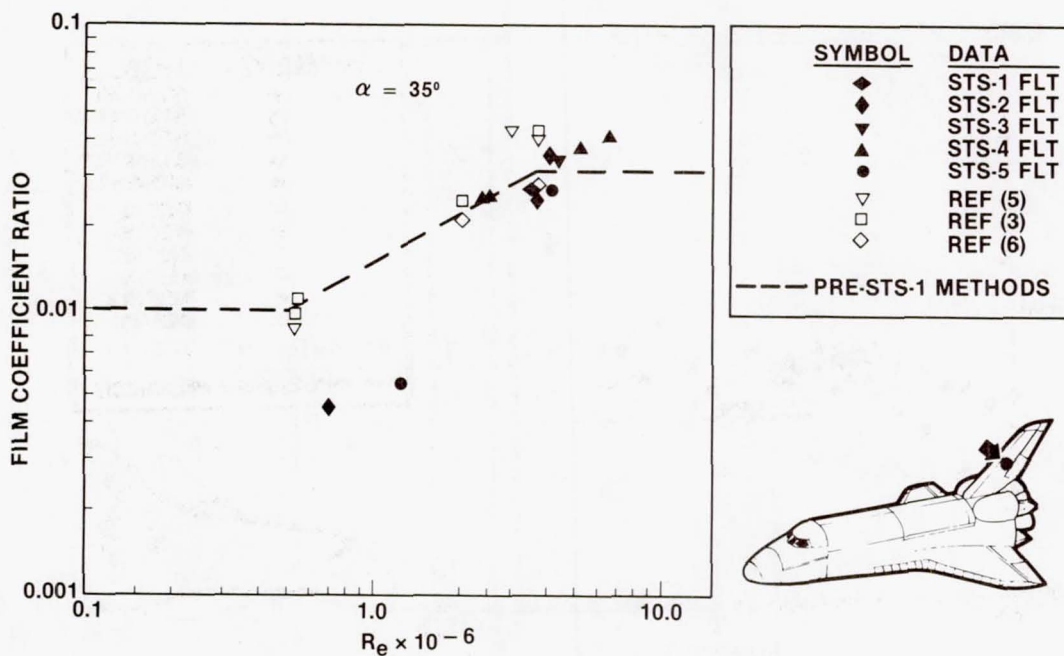
Figure 23.- Concluded.

VERTICAL TAIL CORRELATION V07T9941



(a) $\alpha = 40^\circ$.

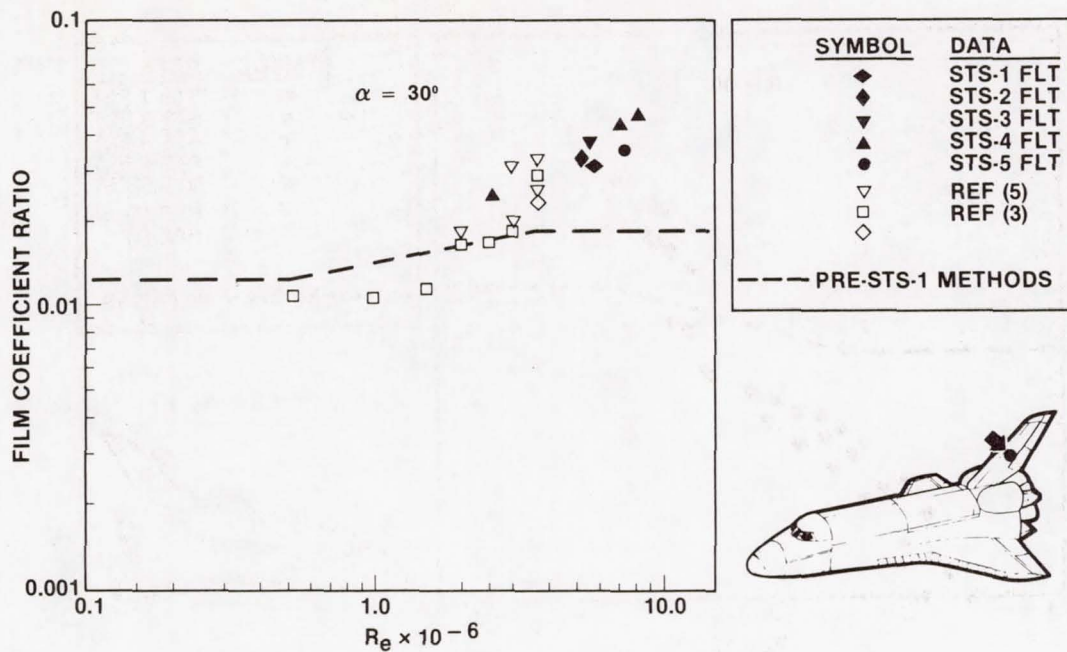
VERTICAL TAIL CORRELATION V07T9941



(b) $\alpha = 35^\circ$.

Figure 24.- Vertical tail correlation.

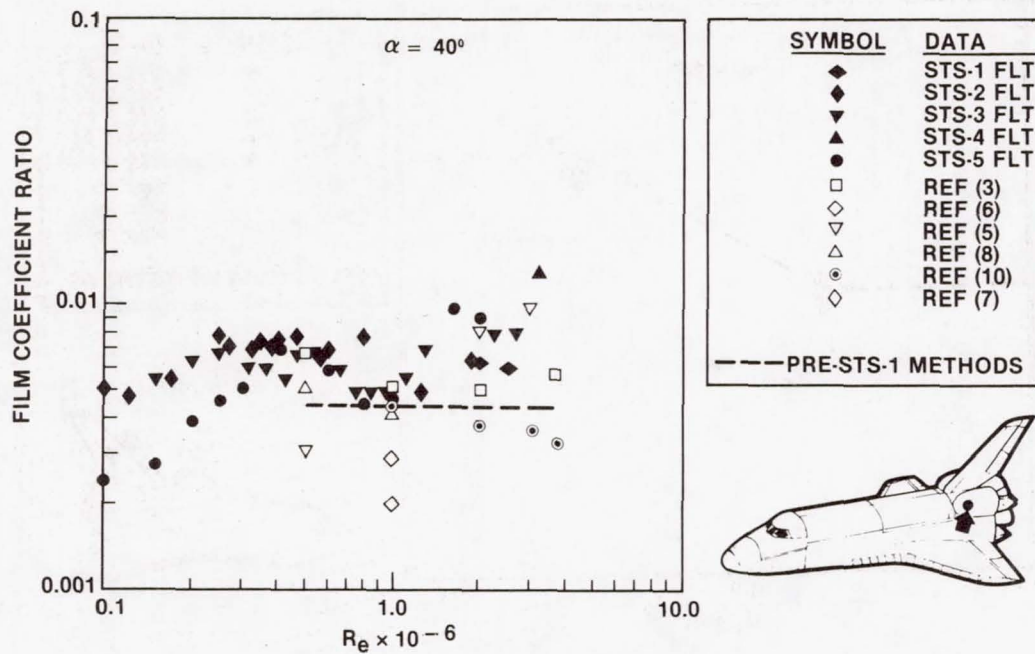
VERTICAL TAIL CORRELATION V07T9941



(c) $\alpha = 30^\circ$.

Figure 24.- Concluded.

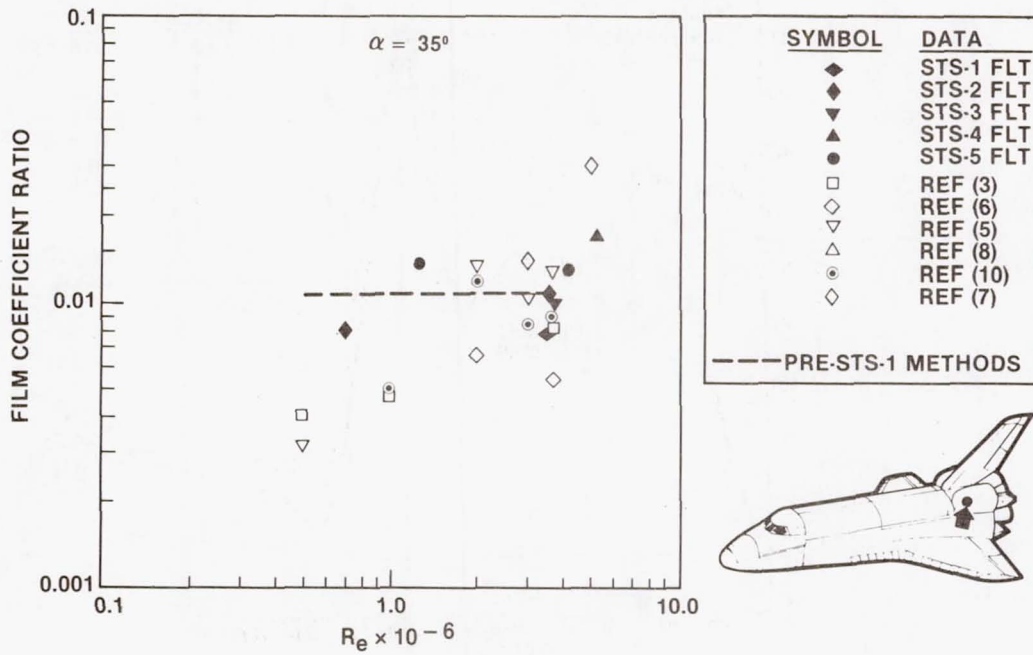
OMS POD HEATING CORRELATION V07T9976



(a) $\alpha = 40^\circ$.

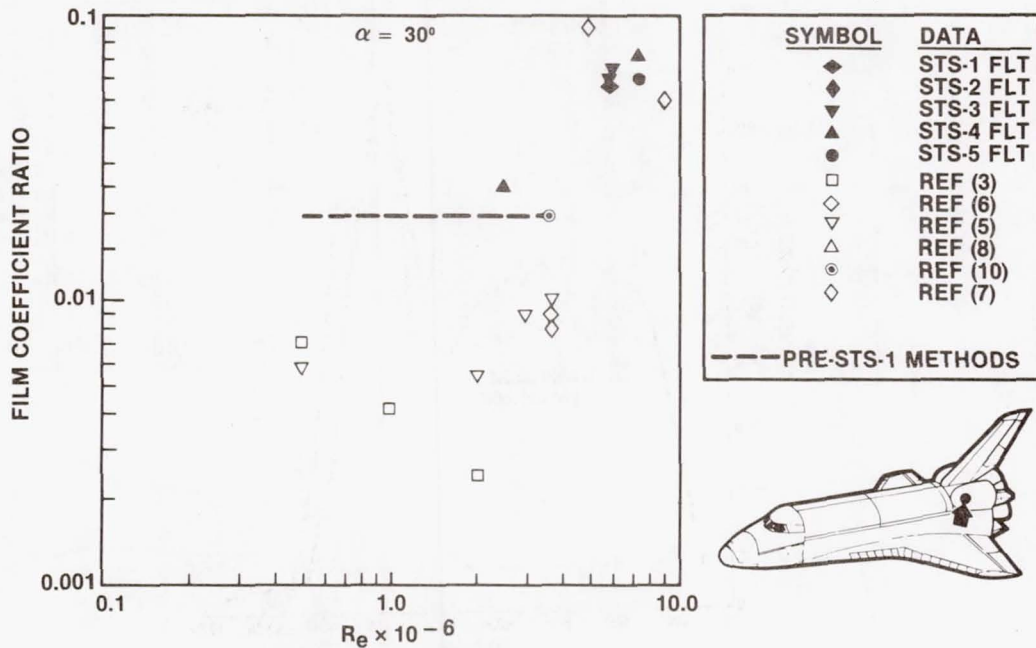
Figure 25.- Orbital Maneuvering System pod heating correlation.

OMS POD HEATING CORRELATION V07T9976



(b) $\alpha = 35^\circ$.

OMS POD HEATING CORRELATION V07T9976



(c) $\alpha = 30^\circ$.

Figure 25.- Concluded.

STS-2 OMS POD TEMPERATURE PROFILES V07T9976A

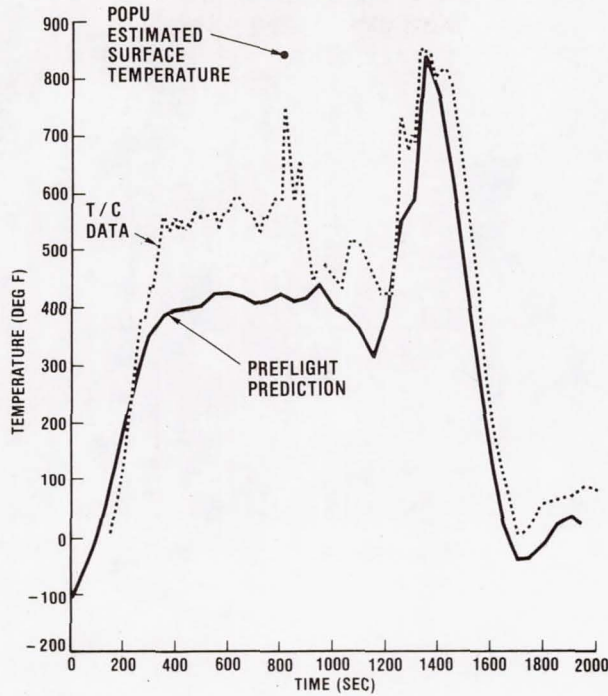


Figure 26.- STS-2 Orbital Maneuvering System pod temperature profiles (V07T9976A).

STS-4 OMS Pod Temperature Profiles V07T9976A

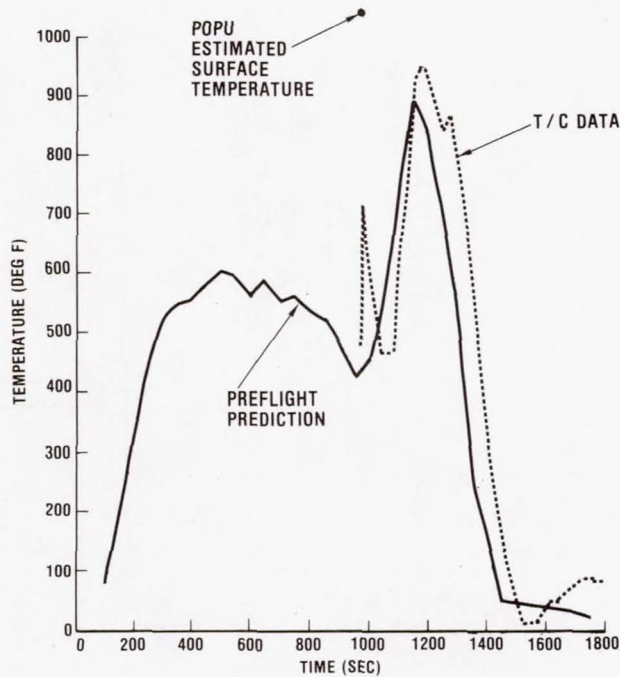


Figure 27.- STS-4 Orbital Maneuvering System pod temperature profiles (V07T9976A).